REPORT DOCUMENTATION PAGE

Form Approved OMB No. 0704-0188

1. REPORT DATE *(DD-MM-YYYY)*	2. REPORT TYPE	3. DATES COVERED *(From – To)*
28-05-2004	Final Report	11 July 2001 - 11-Jul-02

4. TITLE AND SUBTITLE

Deflagration to Detonation Transition Initiation in Pulsed Detonation Engines

5a. CONTRACT NUMBER
F61775-01-WE050

5b. GRANT NUMBER

5c. PROGRAM ELEMENT NUMBER

6. AUTHOR(S)

Dr. R Peter Lindstedt

5d. PROJECT NUMBER

5d. TASK NUMBER

5e. WORK UNIT NUMBER

7. PERFORMING ORGANIZATION NAME(S) AND ADDRESS(ES)

Imperial College Consultants Limited (ICON)
47 Prince's Gate
Exhibition Road
London SW7 2QA
United Kingdom

8. PERFORMING ORGANIZATION REPORT NUMBER

N/A

9. SPONSORING/MONITORING AGENCY NAME(S) AND ADDRESS(ES)

EOARD
PSC 802 BOX 14
FPO 09499-0014

10. SPONSOR/MONITOR'S ACRONYM(S)

11. SPONSOR/MONITOR'S REPORT NUMBER(S)
SPC 01-4050

12. DISTRIBUTION/AVAILABILITY STATEMENT

Approved for public release; distribution is unlimited.

13. SUPPLEMENTARY NOTES

14. ABSTRACT

This report results from a contract tasking Imperial College Consultants Limited (ICON) as follows: It is here proposed to build upon the experience gained and extend ongoing work in two directions. The first is related to the sensitivity of the initial explosion phase to the state of the mixture resulting from injection of the relevant mixture. The second aspect of the proposed work features computations of two-dimensional unsteady flows with comprehensive chemistry and a transported PDF approach closed at the joint scalar level. The contractor proposes the evaluation of a computational approach in the context of the computation of time-dependent compressible flows in two spatial dimensions. Such computations constitute an essential step in the direction of establishing an ability to model Deflagration to Detonation Transition (DDT) in the context of PDEs and are exceptionally resource intensive. Although, a limited study is here proposed to be accomplished (due to funds limitations), it is expected that significant information will be gained!

15. SUBJECT TERMS

EOARD, Fuels, Pulsed Detonation Engines (PDE), Combustion, Detonation

16. SECURITY CLASSIFICATION OF:			17. LIMITATION OF ABSTRACT	18, NUMBER OF PAGES	19a. NAME OF RESPONSIBLE PERSON
a. REPORT	b. ABSTRACT	c. THIS PAGE			WAYNE A. DONALDSON
UNCLAS	UNCLAS	UNCLAS	UL	38	19b. TELEPHONE NUMBER *(Include area code)* +44 (0)20 7514 4299

Imperial College
London
Consultants

Deflagration to Detonation Transition Initiation in Pulsed Detonation Engines

Report reference: F61775 - 01 – WE050
Date: 20 April 2004

Final report for
EOARD

Prepared by
Professor R P Lindstedt

On behalf of
IC Consultants Ltd

Problem Solving • Scientific Services • Expert Advice

Final Report on Contract F61775-01-WE050 Submitted to the European Office of Aerospace Research and Development (EOARD)

Deflagration to Detonation Transition Initiation in Pulsed Detonation Engines

Date Submitted:	20/04/04 Contract F61775-01-WE050
Organization	Imperial College Consultants Limited, 47 Prince's Gate, Exhibition Road, London SW7 2QA, UK
Type of Organisation	A firm of consultants wholly owned by Imperial College.
Principal Investigator Contact Details	Prof. R.P. Lindstedt Imperial College of Science, Technology and Medicine, Department of Mechanical Engineering Exhibition Road, London SW7 2BX, UK. email p.lindstedt@ic.ac.uk; telephone 020 – 7594 7039; fax 020 – 7589 3905.

SUMMARY

Pulsed Detonation Engines (PDEs) cover an unusually wide range of physics and thermochemistry. The flow is time-dependent and compressible and the chemical structure of the fuel has been shown experimentally to have a leading order influence on the transition process. Topics of direct relevance to device design include fuel mixture injection and obstacle enhanced localised turbulent explosions. The latter should result in a transition to detonation and propagation of the resulting wave. Calculation methods – though more rarely adequate chemistry descriptions – exist for laminar shockwave containing flows and the work performed here is aimed to study events leading up to the crucial DDT phase. During the latter a significant fraction of the total cycle time may be expended with the less reactive fuel-air mixtures targeted in practical applications. Work to date has shown that the creation of the initial explosion kernel is strongly dependent upon the state of the mixture at ignition and the duration of the injection phase. Work performed in an earlier contract F61775-00-WE054 has shown that limiting expressions in the high Damköhler number regime, combined with closures at the second moment level for velocity and scalar fields, can reproduce comparatively detailed experimental data with reasonable accuracy. It was also noted that in the key initial phase the alternative limiting source term forms essentially bracketed experimentally observed trends. Work on the same contract also showed that large scalar space transported PDF approaches can capture key aspects of premixed parabolic turbulent flames at high Reynolds numbers.

The work reported here, as part of the current contract (F61775 - 01-WE050) extends the past effort in two directions. The first is related to the sensitivity of the initial explosion phase (prior to DDT) to the state of the mixture resulting from injection of the reactant mixture. The work naturally highlights the need to reconcile the limiting source term closures controlling the heat release as outlined in previous work. The second aspect of the current work features computations of two-dimensional elliptic unsteady flows with comprehensive chemistry and a transported PDF approach closed at the joint scalar level. This part of the work is exceptionally resource intensive and constitutes an essential "proof of concept" study aimed at providing a computational procedure in which the chemistry of the fuel appears in a closed form. The study requires significant computational resources and the test case has therefore been chosen to draw on related work in order to be computationally tractable within the current framework. The results obtained illustrate that the approach is technically possible and constitutes a potential route for dealing with the chemical kinetic effects associated with detonation initiation in a strongly turbulent flow field. However, it must be

recognised that more extensive studies are required. Permission to compute the actual geometry via ITAR/Export Controlled information permission had to be abandoned in favour of generic calculations exploring the influence of turbulence levels on the strength and timing of the onset of the DDT process. The results show a strong influence and indicate a possible solution to the problem of detonation initiation. It is, however, also recognised that computations of the sort attempted stretch our current understanding of turbulent combustion to the limit. Accordingly, experimental studies that can further highlight the physics are strongly recommended.

WORK PROGRAMME

TASK 1: THE SENSITIVITY OF THE EXPLOSION PHASE TO THE STATE OF THE MIXTURE RESULTING FROM INJECTION OF REACTANTS.

Significant new work aimed at reconciling past efforts in the area of the application of higher moment based methods to turbulent gaseous explosions have been performed. The results and methodology are outlined in Appendix A and attached to the current final report. The enclosed appendix has appeared in "CONFINED DETONATIONS AND PULSED DETONATION ENGINES", Editors G.D. Roy, S.M. Frolov, R.J. Santoro and S.A. Tsyganov, Torus Press, Moscow, 2003. The final task of the current project, the computation of geometries of direct relevance to current development work on PDE engines, had to be deleted due to an absence of ITAR/Export Controlled information clearance. The work outlined below has been substituted in order to explore the influence of initial turbulence on the strength of the initial DDT kernel.

EFFECTS OF INITIAL TURBULENCE ON THE TIME EVOLUTION OF EXPLOSION KERNELS

The calculation method outlined in Appendix A features closures at the second moment level for velocity and scalar fields. The "return to isotropy" and "strain" redistribution parts are obtained from model formulations derived in constant density flows. The model used here is that of Haworth and Pope (1987) which is based on a stochastic Lagrangian Generalized Langevin Model (GLM). The latter features a non-linear return to isotropy and has been calibrated and tested for a range of homogeneous turbulence and free shear flows. An important feature of the model is that it also yields a closure for the pressure scrambling term in the scalar flux equation and thus allows for realizable modelling of both pressure strain correlations.

$$\phi_{ij} = \bar{\rho}\left[\frac{\tilde{\varepsilon}}{\tilde{k}}C_{ij}[\mathbf{b}] + B_{ijkl}[\mathbf{b}]\frac{\partial \tilde{u}_k}{\partial x_l}\right]\tilde{k} = \bar{\rho}\,G_{ik}\,\widetilde{u_k'' u_j''} + \bar{\rho}\,G_{jk}\,\widetilde{u_k'' u_i''} + \bar{\rho}(C_w + \frac{2}{3})\delta_{ij}\,\tilde{\varepsilon} \tag{1}$$

$$\phi_{ic} = \bar{\rho}\left[\frac{\tilde{\varepsilon}}{\tilde{k}}C^c_{ij}[\mathbf{b}] + B^c_{ijkl}[\mathbf{b}]\frac{\partial \tilde{u}_k}{\partial x_l}\right]\widetilde{u_j'' c''} = \bar{\rho}\,G_{ik}\,\widetilde{u_k'' c''} - \bar{\rho}\frac{\tilde{\varepsilon}_c}{\tilde{c''^2}}\widetilde{u_j'' c''} \tag{2}$$

However, in turbulent premixed flames, the "production" by strain is not the principal cause of anisotropy and it has been pointed out by Lindstedt and Vaos (1999) that, regardless of specific model formulations, the rate at which energy is transferred between components is substantially lower than the rate at which anisotropy is produced. Instead, the dominant influence is from the mean pressure gradient terms Φ_{ij} and Φ_{ic} associated with preferential acceleration effects.

$$\Phi_{ij} = -\left[\overline{u_i''}\frac{\partial \bar{p}}{\partial x_j} + \overline{u_j''}\frac{\partial \bar{p}}{\partial x_i}\right] \qquad \Phi_{ic} = -\overline{c''}\frac{\partial \bar{p}}{\partial x_i} \tag{3}$$

The potential importance of terms of the above type is obvious in environments with strong pressure gradients. Furthermore, the current model for redistribution should also include the contribution from preferential acceleration effects. The functional forms are given below.

$$\phi_{ij}^{2} = \phi_{ij}^{CD} + \phi_{ij}^{A} \qquad \phi_{ij}^{A} = -\left[A_{ij}^{1}[\mathbf{b},\mathbf{u}''] + A_{ij}^{1}[\mathbf{b},\overline{\mathbf{u}''}] \right] \overline{\rho} a_k$$

(4)

$$\phi_{ic}^{2} = \phi_{ic}^{CD} + \phi_{ic}^{A} \qquad \phi_{ic}^{A} = \left[A_{ic}[\mathbf{b},\overline{\mathbf{c}''}] \right] \overline{\rho} a_k \qquad a_k = -\frac{1}{\overline{\rho}} \frac{\partial p}{\partial x_k}$$

The isotropization of production (IP) model is adopted for the closure of the tensor $\boldsymbol{A}$. The model applied here is zeroth order in the anisotropy tensor:

$$A_{ij}^{1}[\mathbf{b},\overline{\mathbf{u}''}] = \frac{2}{5}\delta_{ik}\overline{\mathbf{u}_j''} - \frac{1}{10}\left(\delta_{ij}\overline{\mathbf{u}_k''} + \delta_{jk}\overline{\mathbf{u}_i''}\right) \qquad \phi_{ij}^{A} = -0.3\left(\Phi_{ij} - \frac{1}{3}\delta_{ij}\Phi_{kk}\right)$$

(5)

$$A_{ic}[\mathbf{b},\overline{\mathbf{c}''}] = \frac{1}{3}\delta_{ik}\overline{\mathbf{c}''^2} \qquad \phi_{ic}^{A} = -\frac{1}{3}\Phi_{ic}$$

The inclusion of terms of the above type into calculation procedures is non-trivial due to the complex mathematical forms. The fractal based model of Lindstedt and Vaos (1999) has been extended by Kuan *et al.* (2003), as shown in Appendix 1, to encompass strongly turbulent flows and it has been shown that the model can reproduce explosion kernels with overpressures in excess of 160 kPa.

$$\overline{S}_c = \overline{\rho} C_1 \frac{\tilde{\varepsilon}_c}{\tilde{c}''^2} \tilde{c}(1-\tilde{c}) \cong \overline{\rho} C_1 \left[1 + C_2 \frac{\rho_u}{\overline{\rho}} \frac{u_t}{v_k} \right] \frac{\tilde{\varepsilon}}{\tilde{k}} \tilde{c}(1-\tilde{c}) \tag{6}$$

The constants C_1 and C_2 have been calibrated to the values of 2.6 and 1.2 on the basis of flames stabilized in an opposed jet geometry (Lindstedt and Vaos 1999). The velocity reaction rate correlation term is closed through the assumption of a bimodal PDF and the thermochemistry (eg. laminar burning velocities) has been obtained through the simulation of laminar flames using detailed chemistry.

RESULTS

As shown in Appendix A, good agreement can be obtained with experimental data for the base case with low initial turbulence levels. Increasing the initial turbulence levels, achievable in practice through a variety of means, has a strong impact upon both the explosion over-pressure and the time taken to reach this point. The predicted pressure traces shown in Figures 1.1 and 1.2 corresponds to initial turbulence fields of u" = 1, 10 and 25 m/s.

For the current rather weakly reacting stoichiometric methane-air mixtures, the time to explosion can be reduced from around 50 ms to 10 ms with an increase in the turbulence intensity from 1 m/s to 25 m/s. It is worth observing that the predominant delay is caused by the initial flame travel of close to 0.5 m before the single obstacle is reached (see Appendix A). Turbulence velocities of the order 25 m/s should be comparatively readily achieved in a PDE given the amount of flow that can be generated through diverting some of the energy of each detonation pulse. A remaining principal difficulty is to assess the influence of turbulent quenching via strain and direct chemical

kinetic effects during the DDT phase under such conditions and further experimental and supporting theoretical work remains necessary.

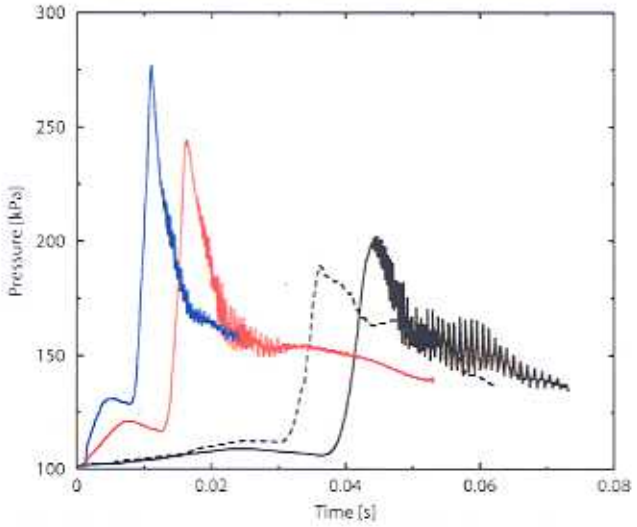

Figure 1.1 Comparison of computed and measured (dashed line) pressure traces at the location of the obstacle (0.478 m) for turbulent gaseous explosions in pre-existing turbulence fields. The black lines, red lines and blue lines represent calculations with initial turbulence fields of u" = 1, 10 and 25 m/s respectively.

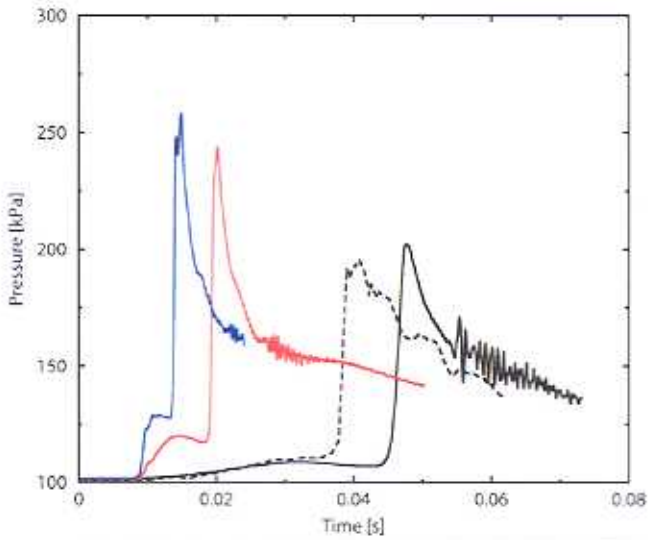

Figure 1.2 Comparison of computed and measured (dashed line) pressure traces downstream of the obstacle (3.208 m) for turbulent gaseous explosions in a pre-existing turbulence fields. The black lines, red lines and blue lines represent calculations with initial turbulence fields of u" = 1, 10 and 25 m/s respectively.

The corresponding velocity field predictions are shown in Figures 1.3 to 1.6. The profile shapes and magnitudes of the mean velocities illustrate the strong influence of the initial turbulence field upon the temporal evolution. The very strong pressure and velocity fluctuations present are evident both in the

pressure traces of Figures 1.1 and 1.2 and in the mean velocities shown in Figures 1.3 and 1.4. The initial dip in the axial velocity profiles correspond to the peak pressure of Figure 1.1 and marks the onset of explosion. With higher initial turbulence levels, the strength of the explosion increases and this is reflected in the magnitude of the flow acceleration at the onset of the explosion.

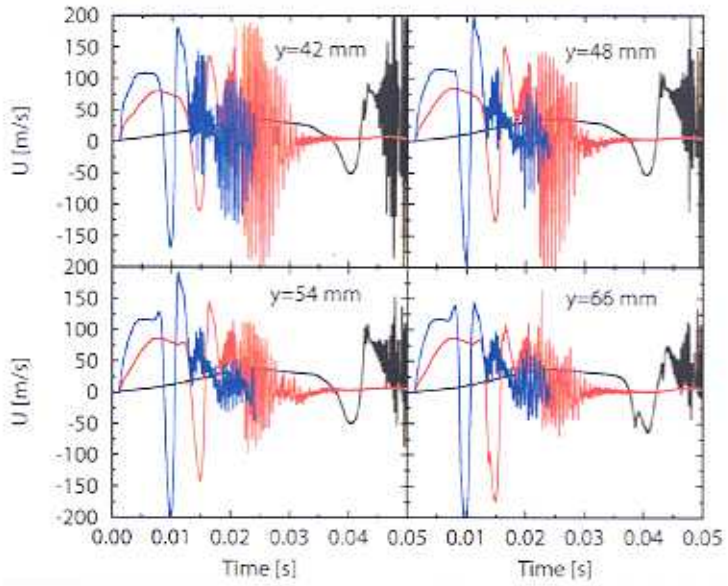

Figure 1.3 Comparison of computed and measured (symbols) axial mean velocities at the location of the obstacle for turbulent gaseous explosions in pre-existing turbulence fields. Lines are as in Figure 1.1

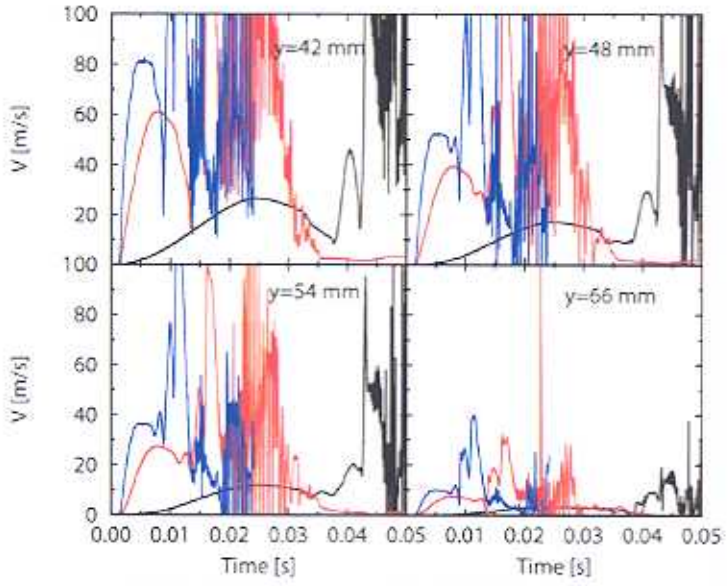

Figure 1.4 Comparison of computed and measured (symbols) cross-stream mean velocities at the location of the obstacle for turbulent gaseous explosions in pre-existing turbulence fields. Lines are as in Figure 1.1.

The significant increase in turbulence levels is also well illustrated in Figures 1.5 and 1.6. However, significant caution is required in interpreting such traces given the extreme complexity of the flow

field. Nevertheless, it is worth observing that for the case where experimental data is available, surprisingly good agreement is obtained as shown in Appendix A.

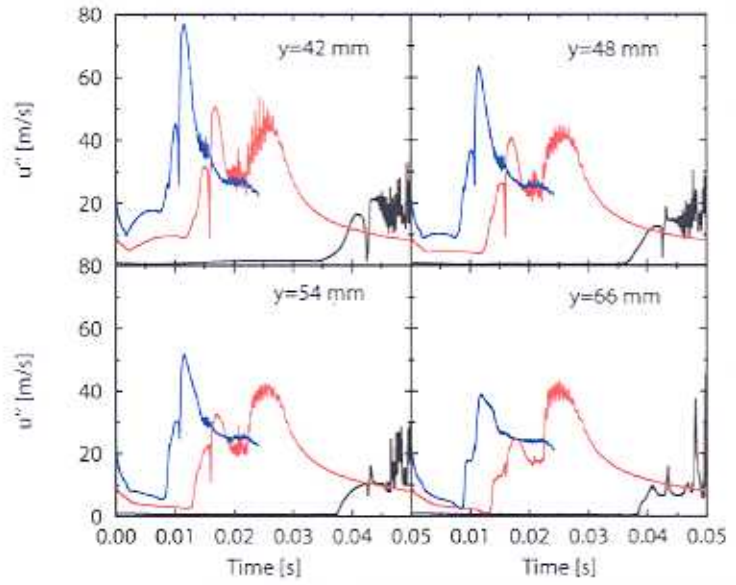

Figure 1.5 Comparison of computed and measured (symbols) axial turbulence velocities at the location of the obstacle for turbulent gaseous explosions in pre-existing turbulence fields. Lines are as in Figure 1.1.

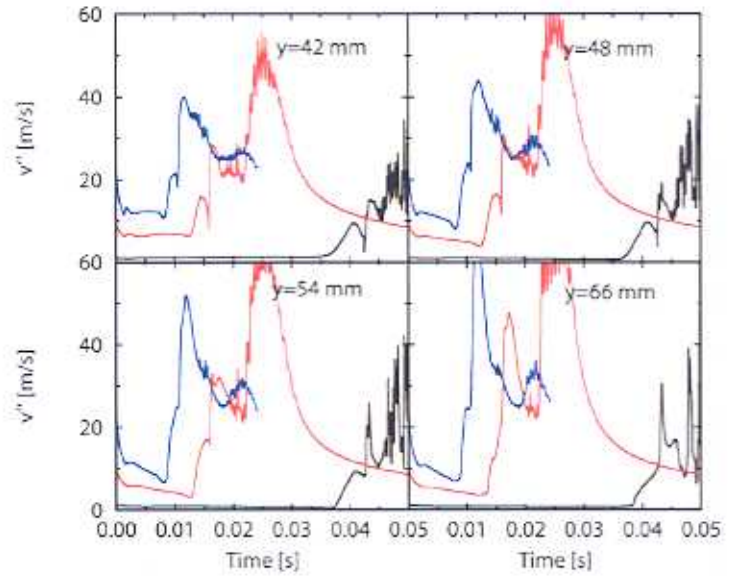

Figure 1.6 Comparison of computed and measured (symbols) cross-stream turbulence velocities at the location of the obstacle for turbulent gaseous explosions in pre-existing turbulence fields. Lines are as in Figure 1.1

DISCUSSION

The results shown above illustrate the strong influence of initial turbulence levels upon the evolution of the explosion kernel. A main benefit of the use of turbulence to enhance the DDT process is a reduction in the relative sensitivity to the reactivity of the fuel. The drawback is that the turbulence intensities and scales have to be such that rapid flame propagation is promoted without undue quenching due to turbulence – a difficult balance to obtain. From a theoretical perspective it is important to point out that no attempt to model such effects in a rigorous manner has been reported in the literature to date. As a first step, the possibility of performing transient transported PDF calculations is assessed in the section below. It must, however, be emphasized that carefully controlled experimentation is necessary given the extreme complexities associated with the flows.

TASK 2: FURTHER EVALUATION OF THE POTENTIAL OF TRANSPORTED PDF APPROACHES IN THE CONTEXT OF TIME DEPENDENT CALCULATIONS.

Work on Task 2 centered on the extension of the high Reynolds number parabolic transported PDF calculations, reported as part of the earlier contract F61775-00-WE054, to include elliptic time-dependent cases where boundary conditions result in large scale flow instabilities. The predominant concern here is the validation of the calculation procedure within the resources available. Furthermore, due to the need for detailed comparisons with measurements, computations have therefore been preformed for bluff body stabilized flames at a range of Reynolds numbers. The fuel featured to date comprises of a mixture of natural gas and hydrogen. The flame under consideration here is the axi-symmetric bluff body stabilized diffusion flame investigated extensively over many years by Masri and co-workers at the University of Sydney (e.g. Dally *et al.* 1998). The burner geometry and layout is shown below. Time-dependent calculation of the type presented here are exceptionally resource demanding. Indeed, the "proof of concept" calculations shown here are probably the most comprehensive performed to date.

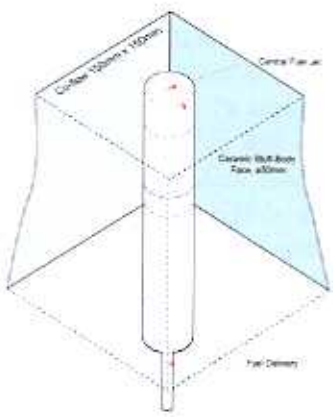

Figure 2.1 The experimental burner configuration used by Dally *et al.* (1998)

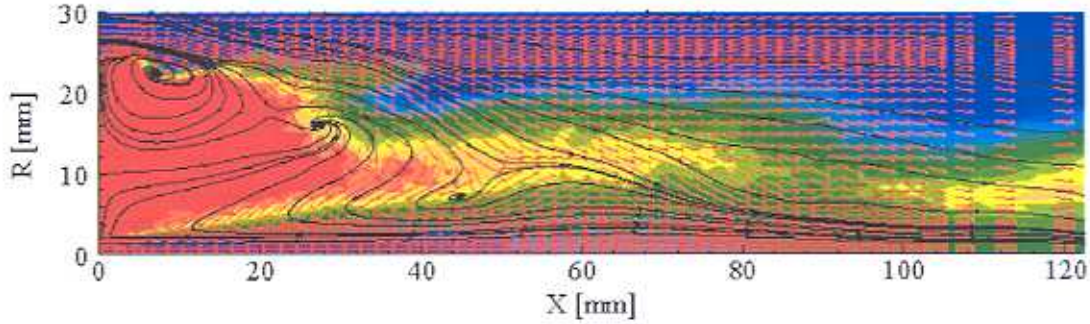

Figure 2.2
Instantaneous velocity and temperature fields for the Sydney bluff body burner flame denoted HM1 obtained through the current unsteady RANS computation coupled with a transported PDF approach closed at the joint scalar level for the thermochemistry.

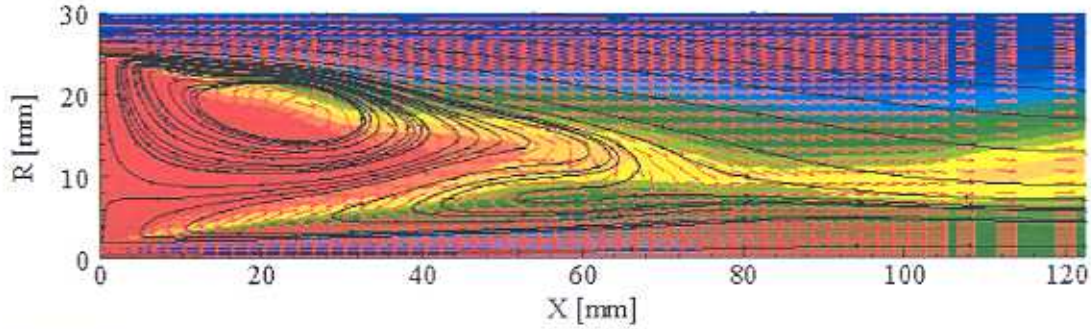

Figure 2.3
Averaged velocity and temperature fields for the Sydney bluff body burner flame denoted HM1 obtained through the current unsteady RANS computation coupled with a transported PDF approach closed at the joint scalar level for the thermochemistry.

The flow is unsteady and elliptic and the equation set and solution technique for the flow field is as given in Appendix A with the key extension that a transported PDF approach with a scalar space of 16 independent, 4 dependent and 28 steady state species is applied to close the thermochemistry. The chemistry applied is identical to that of the parabolic jet flame studied earlier by Lindstedt *et al.* (2000). The same time-dependent elliptic calculation procedure featuring a second order accurate TVD scheme on a staggered grid is used in both cases. The calculation is performed is a two-dimensional axisymmetric geometry with a distributed 124x109 computational grid. Good temporal resolution is maintained with a Courant number not exceeding 0.1 for the finite volume part of the computation. The solution procedure for the PDF equation features between 200 and 400 moving Lagrangian particles per cell. In addition, a variable number of steps are used to integrate the PDF equation during each finite volume step and the mean density field is filtered before it is passed to the finite volume solver. A key point of interest is the evident ability of the approach to correctly identify the large scale instability in the upper shear layer observed experimentally. The very significant differences between a realization of the instantaneous and averaged velocity fields is readily apparent through a comparison of Figures 2.2 and 2.3. The resulting mean velocity fields, extracted by averaging the calculation for part (~ 50%) of an instability cycle time can be seen in Figures 2.4 to 2.7. It is important to note that resource limitations precluded a full integration over several instability cycles and the results shown in Figure 2.4 to 2.11 are therefore principally used for illustration purposes and to provide comparisons with subsequent calculations.

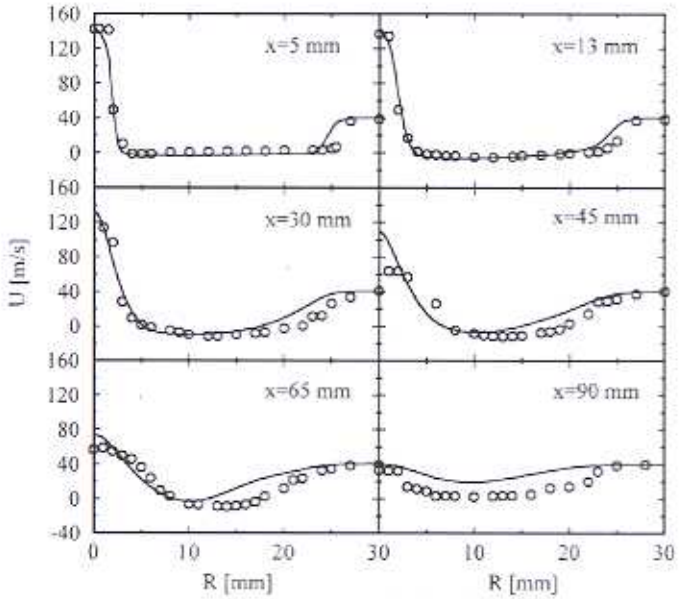

Figure 2.4
Averaged axial velocities for the Sydney bluff body burner flame denoted HM1 obtained through the current unsteady RANS computation coupled with a transported PDF approach closed at the joint scalar level for the thermochemistry.

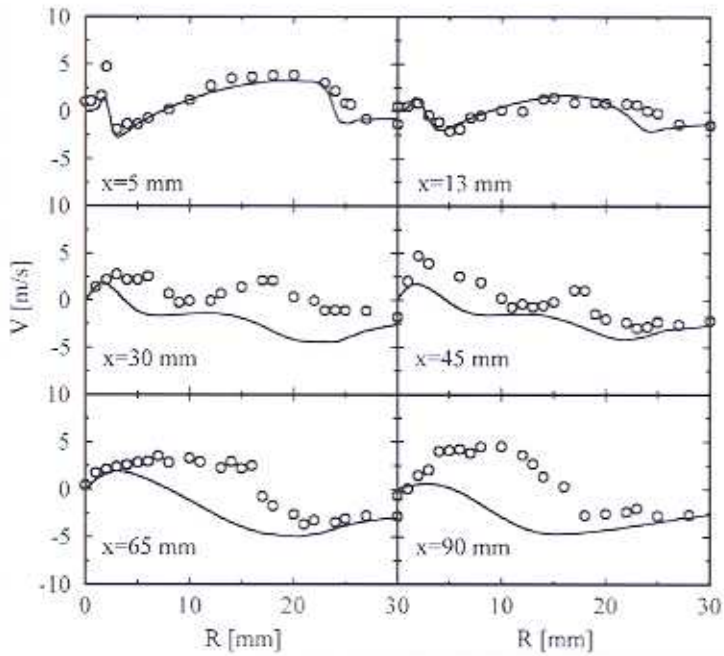

Figure 2.5
Averaged cross-stream velocities for the Sydney bluff body burner flame denoted HM1 obtained through the current unsteady RANS computation coupled with a transported PDF approach closed at the joint scalar level for the thermochemistry.

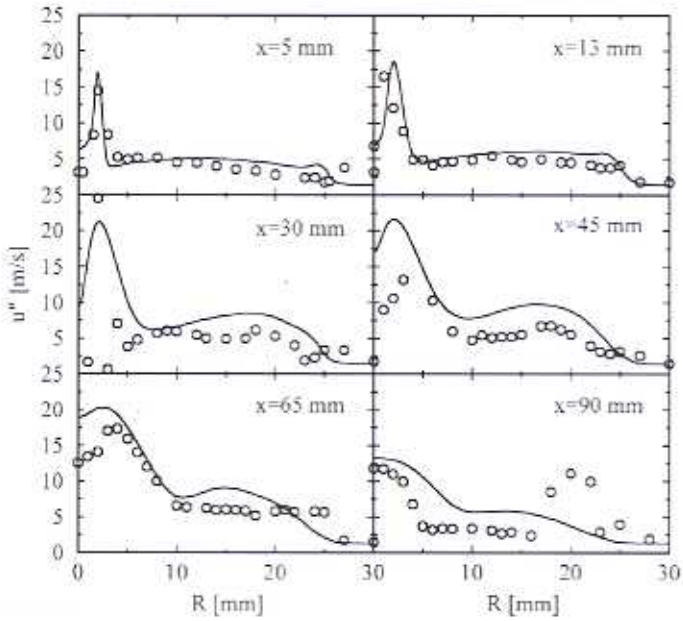

Figure 2.6
Axial turbulence velocities for the Sydney bluff body burner flame denoted HM1 obtained through the current unsteady RANS computation coupled with a transported PDF approach closed at the joint scalar level for the thermochemistry.

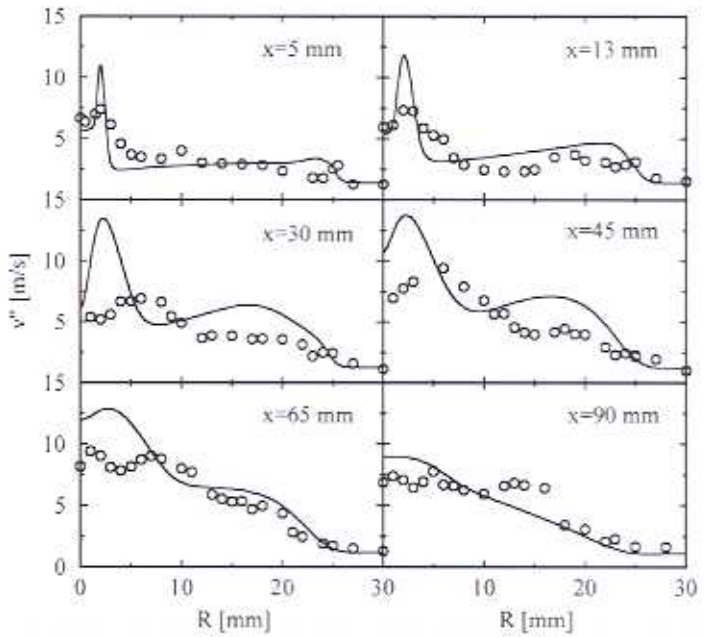

Figure 2.7
Cross-stream turbulence velocities for the Sydney bluff body burner flame denoted HM1 obtained through the current unsteady RANS computation coupled with a transported PDF approach closed at the joint scalar level for the thermochemistry.

The solution of the PDF transport equation (with a closure at the joint scalar level) is obtained, as stated above, using Lagrangian stochastic particles and the modified Curl's mixing model. The current fuel is CH_4/H_2 (1:1) and the jet velocity is 118 m/s (HM1E) with a coflow velocity is 40 m/s. The computation is performed on two networked Intel Xeon 2.2 GHz dual processor Dell Precision 530 workstations using message Passing Interface (MPI) for inter-processor communication and the Scalable Parallel Random Number Generator (SPRNG) for generation of uncorrelated random number streams. Each available processor is assigned an equal number of particles and inter-processor communications required for the computation of the mixing process and compilation of global statistics. The speed-up is 1.94 and 3.84 over two and four processors and the parallel efficiency can be improved further by using a better network configuration. Examples of scalar field predictions are given in Figures 2.8 and 2.9 below. The agreement with respect to the final products of combustion is very reasonable though averaging over several instability cycles, as outlined below, is necessary for full quantitative comparisons with measurements. The results obtained are, however, encouraging. Finally, results obtained for the mean and rms of the mixture fraction are shown in Figures 2.10 and 2.11. The work performed on the coupling of transported PDF methods to transient calculation methods establish beyond doubt that such simulations are possible. The application of this technique to the study of turbulence enhanced DDT is distinctly possible and can be expected to provide a powerful, albeit computationally expensive, tool.

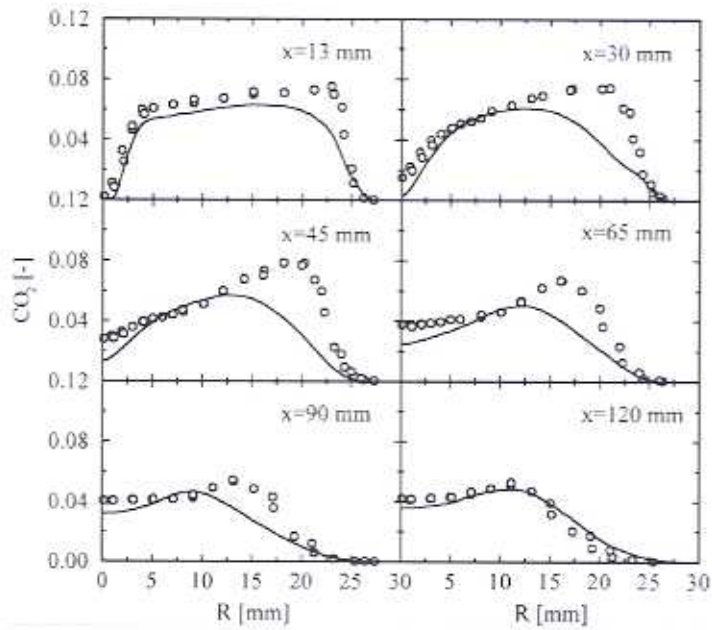

Figure 2.8
Mean carbon dioxide concentrations for the Sydney bluff body burner flame denoted HM1 obtained through the current unsteady RANS computation coupled with a transported PDF approach closed at the joint scalar level for the thermochemistry.

Coupled transient simulations have also been performed covering time-averaging of results covering several instability cycles to enable more reliable comparisons with measurements. Computations were restarted from the uncoupled calculations by Lindstedt and Kuan (2004).

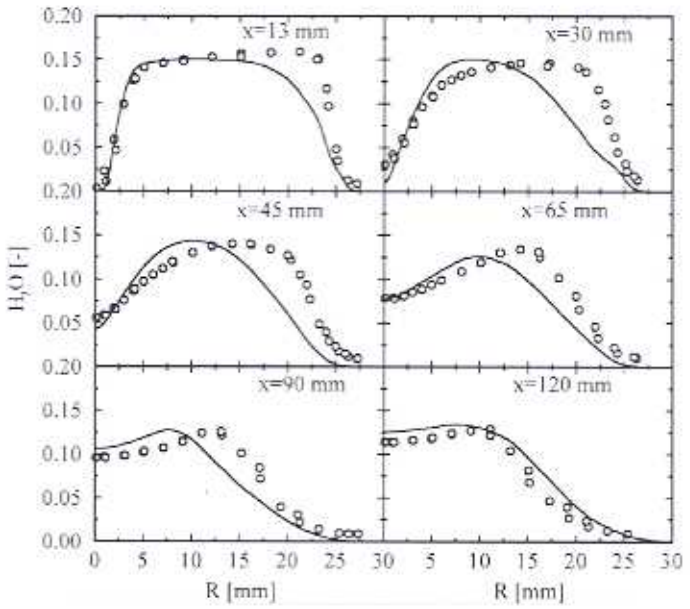

Figure 2.9
Mean water concentrations for the Sydney bluff body burner flame denoted HM1 obtained through the current unsteady RANS computation coupled with a transported PDF approach closed at the joint scalar level for the thermochemistry.

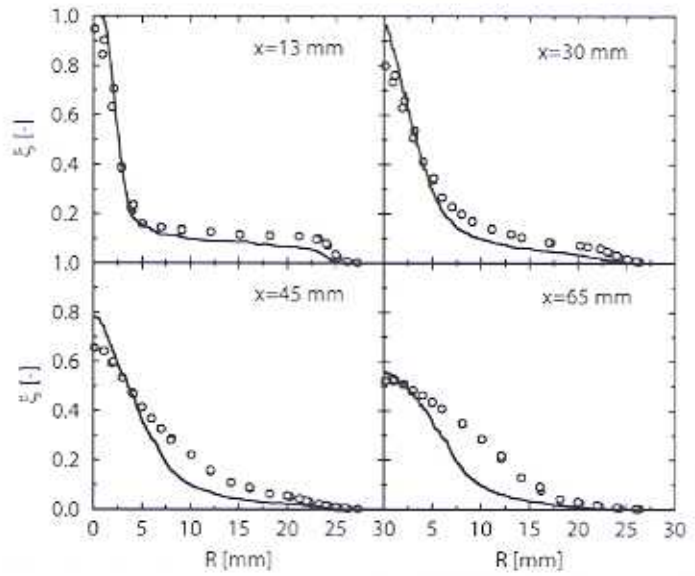

Figure 2.10
Mean mixture fraction profiles for the Sydney bluff body burner flame denoted HM1 obtained through the current unsteady RANS computation coupled with a transported PDF approach closed at the joint scalar level for the thermochemistry.

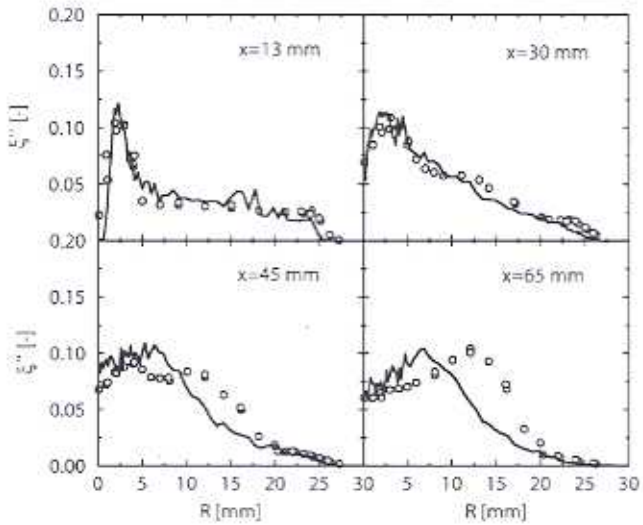

Figure 2.11
RMS mixture fraction profiles for the Sydney bluff body burner flame denoted HM1 obtained through the current unsteady RANS computation coupled with a transported PDF approach closed at the joint scalar level for the thermochemistry.

Time averaging performed according to the simple method by Muradoglu *et al.* (1999) with the density evaluated as

$$\overline{\rho}^{n} = \left(1 - \frac{1}{N_{TA}}\right)\rho^{n-1} + \frac{1}{N_{TA}}\overline{\rho}^{n}$$

where N_{TA} is the under-relaxation factor.

Time averaging is useful in reducing the effects of fluctuations induced by statistical errors in the density field without either increasing the number of stochastic particles or the use of statistical resampling. However, the temporal resolution and the physics of the problem is affected. Smoothing algorithms, such as cross-validated cubic smoothing splines can be problematic particularly in evolving regions with steep gradients. Cross-validated cubic spline techniques use statistical information to determine the amount of smoothing required and thus, are also subject to statistical error. In other approaches, not featuring cross-validation, the degree of smoothing needs to be specified. Furthermore, smoothing does little to improve the statistical accuracy of the data set.

Discrete Monte Carlo sampling converges with a rate proportional to the square root of the number of stochastic particles. The statistical error can be reduced by statistical resampling which can be achieved by increasing the number of Monte Carlo steps (with reduced time step for each Monte Carlo step) within each fractional step of the coupled calculation procedure. The approach reduces the memory requirements but does little to alleviate the computational time required.

Computations with no time averaging shown above illustrate that the directly coupled transient calculation procedure works well in principle. A complication with the calculation reported here is that a larger length scale estimate was applied at the bluff body boundary. This choice of boundary condition results in much more pronounced vortex shedding which strongly affects the upper shear layer and the structure of the recirculation zone. Similar sensitivities have been observed in the LES study of Kempf *et al.* (2004).

Given the uncertainties in the boundary conditions and statistical resolution, a strongly under-relaxed (N_{TA} = 1000) simulation was performed. By comparison, the results shown above in Figure 2.4 to 2.11 were obtained with N_{TA} = 1. The former computations features the same boundary conditions as discussed by Kempf *et al.* (2004). Although Muradoglu *et al.* (1999) used time averaging in the context of a steady state solution procedure, the approach is here extended to a transient calculation. A temporal resolution of the order of 10^{-4} s is arguably required to resolve the periodic fluctuations encountered in the current flow. In the simulation, the time steps are of the order of 10^{-6} s which results in a temporal resolution of the order of 10^{-3} s. Despite the above reservations, a transient behaviour is observed and further details are given below. Evidently, it is desirable to provide better temporal resolution and to reduce statistical errors. The two methods which appear most favourable are to simply increase the number of stochastic particles and/or to use statistical resampling. Better smoothing algorithms may also be useful.

The evolution of the various scalars (temperature and species mass fractions of OH, H_2O, CO, CO_2 and NO) is illustrated through the time histories in Figure 2.12. After an initial time window of approximately 6 ms, regular periodic fluctuations are observed at locations close to the bluff body (x < 60 mm). Further downstream, the flame extinguishes due to large scale fluid structures (see Figure 2.13) after the restart and is still in the process of reigniting. A larger integration time is therefore required and the instantaneous contour plot at 10.8 ms after the restart can be found in Figure 2.14.

The results presented below are averaged over a time window of 4.5 ms beginning 6 ms after the restart. As can be seen from Figure 2.12, 4 periodic cycles with a period of approximately 1.2 ms (833 Hz) can be observed in this time window. The scalar field predictions are compared to measurements in Figures 2.15 - 2.22 for axial locations with x < 65 mm. Results for locations further downstream are not shown as the flame is still developing. The results are similar to that of the uncoupled simulation although the predictions are arguably better at the first three measuring stations. The predicted temperature at x = 65 mm is lower than measurements and, as discussed above, further temporal integration is required.

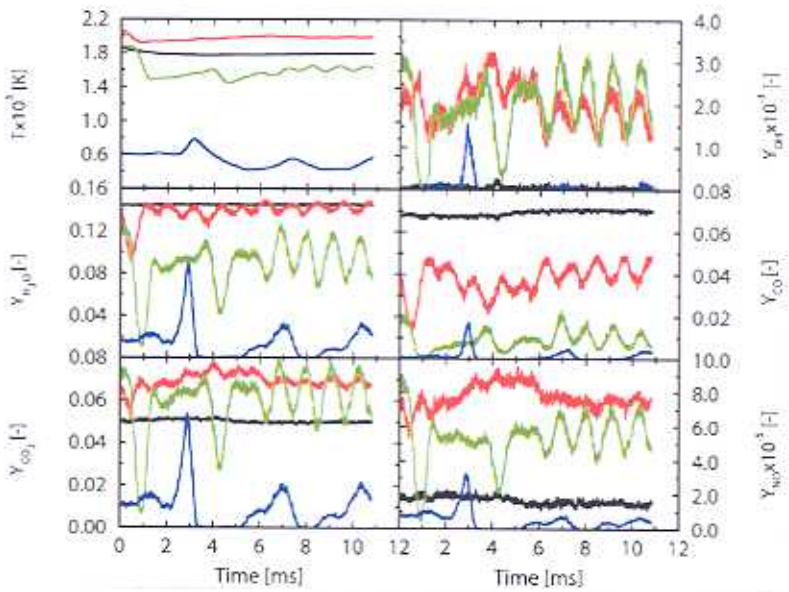

Figure 2.12 Evolution of various scalars after initialization from the uncoupled transported PDF solution. The black, red, green and blue lines represent time histories at locations 1, 2, 3 and 4 respectively as marked in Figure 2.13. In the simulation shown N_{TA} = 1000.

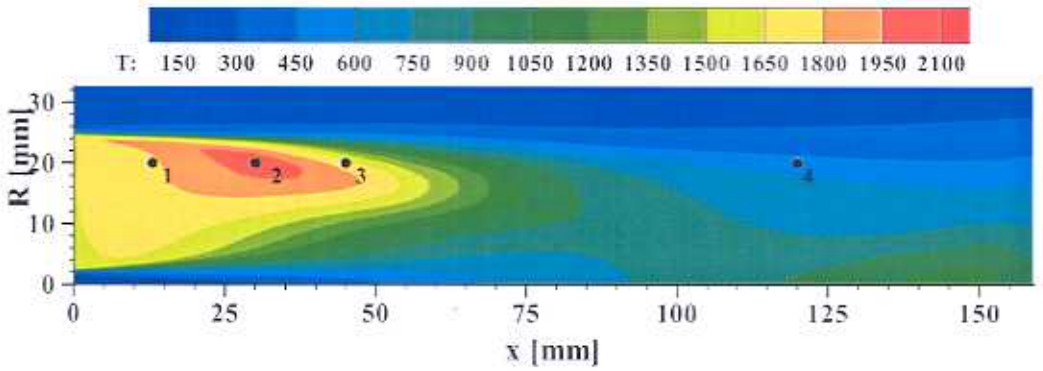

Figure 2.13 Contour plot of the time averaged temperature [K] for flame HM1. The locations correspond to the time histories in Figure 2.12.

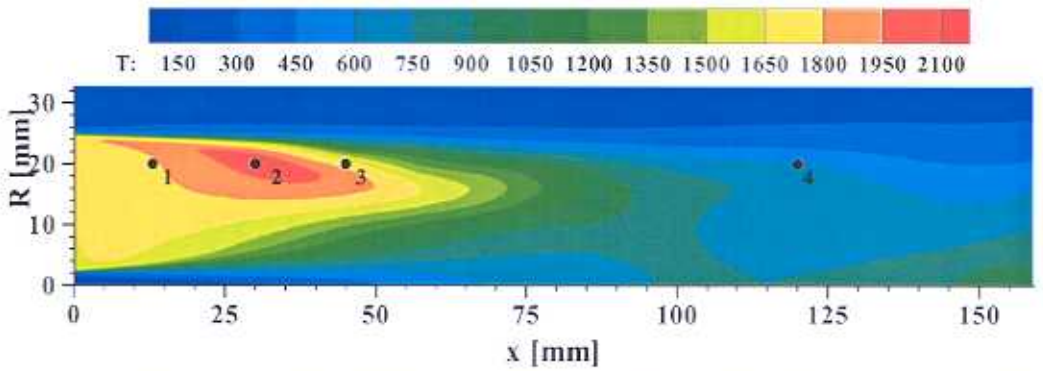

Figure 2.14 Contour plot of the instantaneous temperature [K] for flame HM1 at 10.8 ms after the computation has been restarted. The locations correspond to the time histories in Figure 2.12.

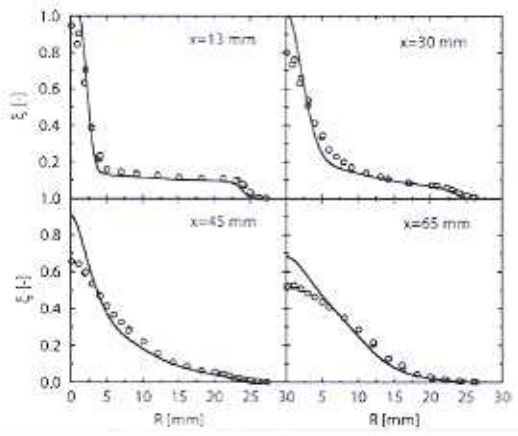

Figure 2.15 Radial profiles of the time averaged mean mixture fraction for flame HM1. The symbols represent experimental data and solid lines predictions.

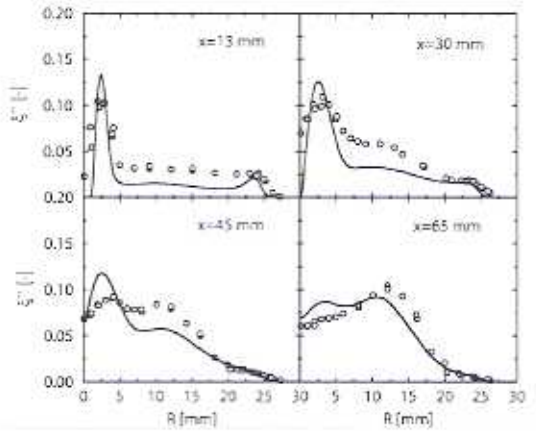

Figure 2.16 Radial profiles of the time averaged mixture fraction rms for flame HM1. The symbols and lines are as in Figure 2.15

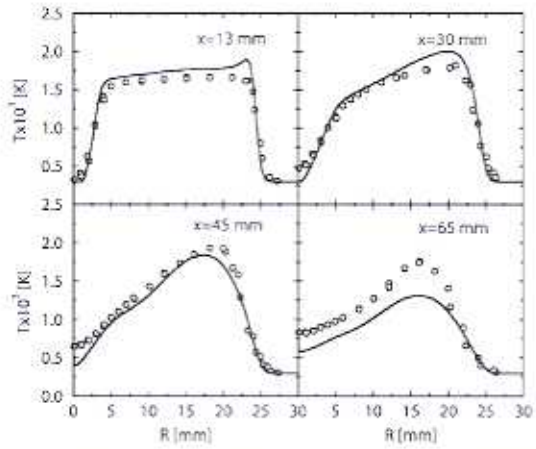

Figure 2.17 Radial profiles of the time averaged temperature for flame HM1. The symbols and lines are as in Figure 2.15.

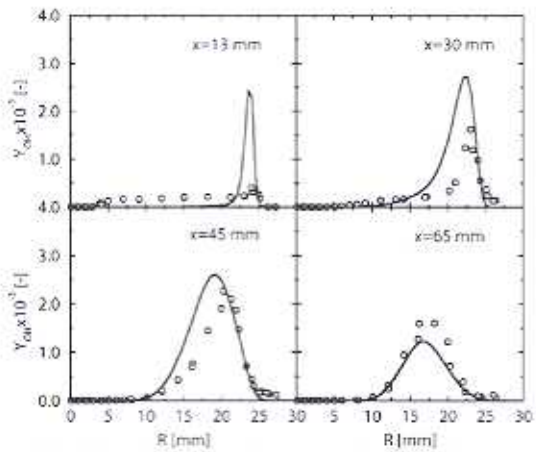

Figure 2.18 Radial profiles of the time averaged OH mass fraction for flame HM1. The symbols and lines are as in Figure 2.15.

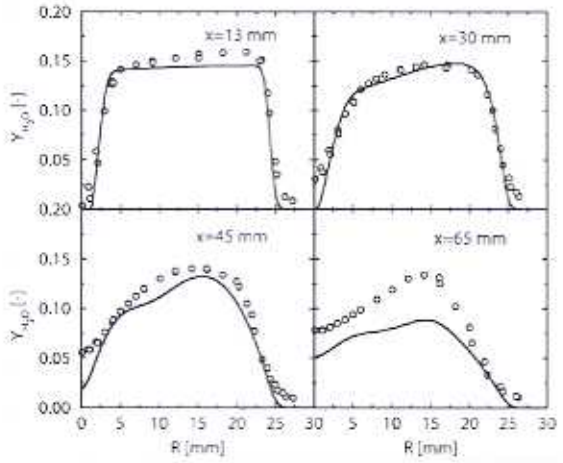

Figure 2.19 Radial profiles of the time averaged H_2O mass fraction for flame HM1. The symbols and lines are as in Figure 2.15

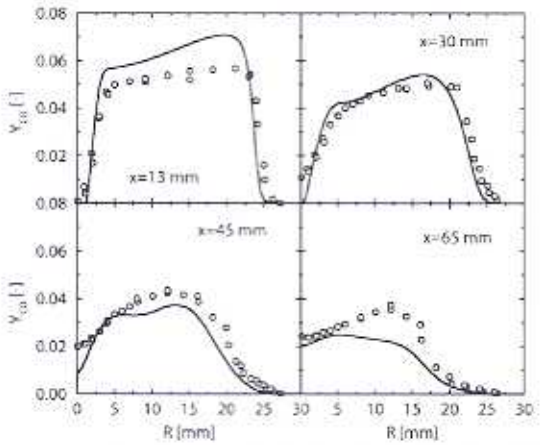

Figure 2.20 Radial profiles of the time averaged CO mass fraction for flame HM1. The symbols and lines are as in Figure 2.15.

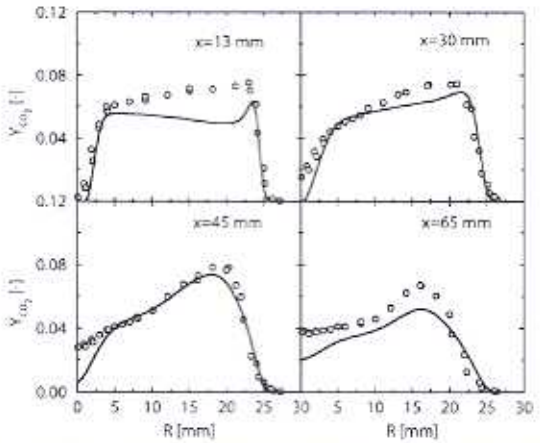

Figure 2.21 Radial profiles of the time averaged CO_2 mass fraction for flame HM1. The symbols and lines are as in Figure 2.15.

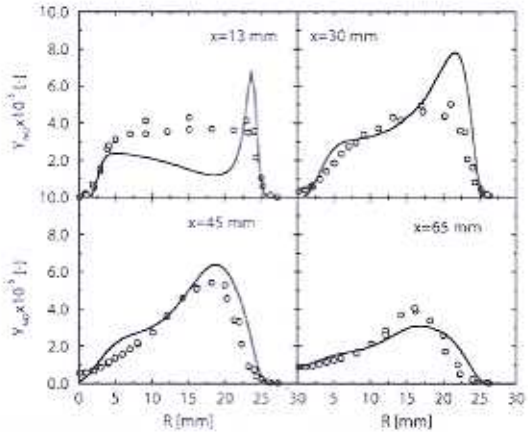

Figure 2.22 Radial profiles of the time averaged NO mass fraction for flame HM1. The symbols and lines are as in Figure 2.15

CONCLUSIONS

The work reported here, as part of the current contract (F61775 - 01-WE050) extends past efforts in two directions. The first is related to the sensitivity of the initial explosion phase (prior to DDT) to the state of the mixture resulting from injection of the reactant mixture. The work naturally highlights the need to reconcile the limiting source term closures controlling the heat release as outlined as part of previous work. The second aspect of the current work features computations of two-dimensional unsteady flows with comprehensive chemistry and a transported PDF approach closed at the joint scalar level for the thermochemistry. This part of the work is exceptionally resource intensive and constitutes an essential "proof of concept" study aimed at providing a computational procedure in which the chemistry of the fuel appears naturally in closed form. The study does require significant computational resources and the test case has therefore been chosen to be computationally tractable within the current framework. The results obtained illustrate that the approach is technically possible and constitutes a potential route for dealing with the chemical kinetic effects associated with detonation initiation in a strongly turbulent flow field. However, it must be recognised that more extensive studies are required. Permission to compute the actual geometry via ITAR/Export Controlled information permission had to be abandoned in favour of generic calculations exploring the influence of turbulence levels on the strength and timing of the onset of the DDT process. The results show a strong influence and indicate a possible solution to the problem of detonation initiation. It is, however, also recognised that computations of the sort attempted stretch our current understanding of turbulent combustion to the limit. Accordingly, experimental studies that can further highlight the physics are strongly recommended.

DEVIATIONS FROM WORKPLAN

The initial delay caused by staffing difficulties with respect to students appeared to be resolved satisfactorily until April 2002 when the student, Mr. G. Colangelo, working on the project had to return to Italy for health reasons. Further delays were caused by the difficulties in obtaining an export license application is being pursued by the Air Force via the EOARD in order to advance the final element of Task 1 - which entailed the computation of geometries of direct relevance to the Air Force.

ACKNOWLEDGEMENT

Despite the technical and other challenges it has been a pleasure to purse the current work and, accordingly, the support of Air Force staff is gratefully acknowledged.

REFERENCES

Dally, B.B., Masri, A.R., Barlow, R.S., Fiechtner, G.J., 1998, Combustion and Flame 114:119-148.

Haworth, D. C. and S.B. Pope. 1987. PDF modeling of self-similar turbulent shear flows. Physics Fluids 30:1026-44.

Kempf, A., Janicka, J. and Lindstedt. R.P. Lindstedt 2004. Efficient Large Eddy Simulation of a Bluff Body Stabilized Non-Premixed Flame, Submitted to Combustion and Flame.

Kuan, T. S., Lindstedt, R.P. and E.M. Vaos. 2003. Higher Moment Based Modeling of Turbulence Enhanced Explosion Kernels in Confined Fuel-Air Mixtures, Advances in Confined Detonations and Pulse Detonation Engines, Torus Press, pp. 17-40.

Kuan, T.S. and Lindstedt, R.P. 2004. Transported Probability Density Function Modelling of a Bluff Body Stabilized Turbulent Flame, To be presented at the 30th Combustion Symposium, Chicago, July 2004.

Lindstedt, R. P. and E.M. Vaos. 1999. Modeling of premixed turbulent flames with second moment methods. Combustion and Flame116:461-85.

Lindstedt, R.P., Louloudi, S.A. and Vaos, E.M. 2000. Jonint Scalar Probability Density Function Modleing of Pollutant Formation in Piloted Turbulent Jet Diffusion Flames with Comprehensive Chemistry. Proc. Combust. Inst. 28:149-156.

Muradoglu, M, Jenny, P., Pope, S.B. and Caughey, D.A., 1999. A Consistent Hybrid Finite-Volume/Particle Method for the PDF Equations of Turbulent Reacting Flows, J. Comp. Phys. 154:342-371.

APPENDIX A

Higher Moment Based Modelling of Turbulence Enhanced Explosion Kernels in Confined Fuel-Air Mixtures

T.S. Kuan, R.P. Lindstedt[1] and E.M. Vaos
Department of Mechanical Engineering
Imperial College of Science, Technology and Medicine
Exhibition Road
London SW7 2BX
UK

ABSTRACT The transition of an initially laminar or turbulent deflagration to a confined gaseous explosion or detonation (DDT) is of fundamental relevance to practical devices such as pulsed detonation engines (PDEs) and remains of key importance to on- and off-shore hazard assessment procedures. The topic is also one of the most challenging in contemporary physics and requires a detailed consideration of the interactions between unsteady high speed turbulent flows and chemical kinetics. Furthermore, in many cases fluid-wall interactions come to the fore. It is therefore perhaps not surprising that the subject has traditionally been treated either on the basis of shock dynamics in laminar flows, typically combined with simplified chemical kinetic expressions, or as a turbulent reacting flow closed at the eddy viscosity level in which the chemistry is considered to be in the high Damköhler number limit. The limitations associated with each approach are obvious and experimental data sets assembled over many decades show - without doubt - that the combined influence of chemistry and flow matters to the DDT process and by implication neither treatment is satisfactory. The current chasm in the theoretical treatment of turbulent gaseous explosions and detonation propagation studies must be bridged in order to provide a technically meaningful modelling capability for turbulence enhanced DDT processes. The focus of the present paper is to use detailed time-resolved experimental data sets to explore the ability of comprehensive moment based closures to reproduce time resolved flow field features up to the point of onset of detonation. A new reaction rate closure is also derived and evaluated. The experimental data set considered features a confined obstacle accelerated premixed turbulent flame of physical relevance to PDEs. Time-resolved mean and rms profiles, obtained using laser Doppler anemometry, are used for comparisons with computational results along with pressure traces and instantaneous spark schlieren photographs. The main conclusions of the study are positive and the work does show that the application of higher moment based closures to model the flow field leading up to the onset of DDT yields surprisingly satisfactory results.

[1] Corresponding author. Email: p.lindstedt@ic.ac.uk; Fax: -44-207-589 3905; Tel: -44-207-594 7039

INTRODUCTION

Calculation methods for transient turbulent reacting flows must balance the fidelity of thermochemical and fluid mechanical closure aspects in order to provide technically useful results. The confined high speed combusting flows considered here are dominated by flow obstacle interactions and present a particular challenge. Chemical reaction occurs in the fine (unresolved) scales and must be modelled irrespective of the technique adopted for the flow field. Furthermore, flow interactions with solid boundaries, e.g. in the context of shock (turbulent) boundary layer interactions, is a severe challenge for both unsteady Reynolds Averaged Navier-Stokes approaches (RANS) and Large Eddy Simulations (LES) even in the absence of chemical reaction. Temporal response issues and flow-field/turbulence interactions with chemistry also occupy central roles during the DDT phase in pulsed detonation engines [1,2] and in emerging propulsion devices in general [3]. The former are, in contrast to the majority of contemporary propulsion devices, intrinsically unsteady and cover an unusually wide spectrum of thermochemistry and physics. Examples of topics of practical relevance include fuel/mixture injection and obstacle (or shock) enhanced localized turbulent explosions resulting in a transition to detonation followed by the propagation of the resulting detonation and its interaction with confinement boundaries.

Key challenges that remain to be resolved during the latter stages of the DDT process include shock interactions with flames and boundary layers. However, two of the principal practical issues at present arguably concern the relative influences of fuel structures and turbulence on the transition process leading up to the actual onset of detonation. The chemical structure of the fuel has been shown experimentally to have a leading order influence on the transition process in smooth tubes [4]. It is also well established that the influence of turbulence reduces the sensitivity of the transition process to the point where alkane fuels, with the exception of methane, show a similar sensitivity. Lower alkenes and alkynes do, however, retain a greater propensity to DDT even in strongly turbulent environments [5]. An exceptionally wide range of turbulence Reynolds numbers is normally encountered during the transition process and the resulting complex interactions between flow and chemistry are likely to play a key role in device design. The resulting demands placed on computational design techniques are severe. Similar issues have for a long time prevailed in the context of hazards related studies of relevance to the modelling of turbulent gaseous explosions. Much of the work in the latter area has been performed in the context of successive studies sponsored by the CEC (DGXII) as part of the Major Technological Hazards Programme and a summary of some of the results has been presented by Arntzen *et al.* [6].

The modelling of turbulent gaseous explosions has to date exclusively featured different variants of closures at the eddy viscosity level. Generally, such closures have only proved adequate when turbulence is driven by local cross-stream gradients. In turbulent reacting flows, by contrast, variable density effects are at least comparable to, and usually outweigh, such generation mechanisms. A consequence of chemical reaction is the occurrence of velocity divergence leading to a reduction of turbulence levels due to the enhanced contribution of the strain components in the normal Reynolds stress "production" terms. However, volume expansion will also result in production through preferential acceleration effects through mean pressure gradient terms in the respective transport equations. Similar considerations apply to the flux vector which may not necessarily be aligned with that of the scalar gradient and therefore result in "non-gradient" transport. Effects of the type outlined above can not be incorporated into eddy viscosity closures. Advantages of higher moment closures are that "history" and convection related effects on the evolution of turbulence are incorporated in a natural manner, while production terms by mean strain components appear in a closed form. Furthermore, effects induced by anisotropy generating mechanisms, such as mean pressure gradients, are also included. Many of the latter features can be expected to be critical for the flows considered here as it may be expected that pressure gradient effects will have a significant impact upon the evolution of turbulence. The application of higher moment based closures to flows with strong pressure gradients is, however, not trivial and presents significant numerical challenges.

In the current context it can also be expected that techniques capable of dealing with direct kinetic effects - with large deviations from equilibrium - will be required in order to model the full DDT process. At present, the transported PDF approach is the only method by which this can be achieved. Hulek & Lindstedt [7] have shown

that one-dimensional transient premixed turbulent flames can be computed with a transported PDF closure at the joint velocity-scalar level. The molecular mixing terms was closed using a binomial Langevin model modified for joint velocity-scalar statistics [8]. Lindstedt & Vaos [9] subsequently explored the effects of different mixing models on the computed turbulent burning velocity and showed that both the binomial Langevin and Curl's mixing models perform well when combined with a closure at the second moment level. In both cases, the chemical reaction rate source term was extracted from laminar flame calculations and reduced to a one-step formulation. Time dependent calculations with realistic (large) scalar spaces (~ 20 independent scalars) are becoming increasingly feasible and are starting to appear [10] though exceptional computational resources are required.

In the present work high Damköhler number techniques are applied to explore the ability of higher moment based closures for the flow field to reproduce major flow field features leading up to the point of onset of detonation. Catlin & Lindstedt [11] have shown that reaction rate expressions based on such assumptions are prone to numerical instabilities at the leading edge of turbulent premixed flames. The result is that the generally accepted leading order scaling between the turbulent burning velocity and turbulent velocity fluctuations is not reproduced in numerical calculations unless a Heaviside function is introduced at the leading edge. A further key observation is that the burning velocity eigenvalue is strongly dependent upon such modifications and that common approaches can be readily expected to lead to errors in excess of 100%. A further observation made is that the turbulent flame brush thickness has to be well resolved computationally in order to ensure physically meaningful results. The adherence to such, comparatively simple, requirements ensures that the intrinsic scaling behaviour of the solved equations is retained. A recent study by Colangelo & Lindstedt [12] has shown that the temporal evolution of gaseous explosions can be captured with useful accuracy and that alternative reaction rate closures based on a fractal assumption with the limiting cases of inner cut-off scales corresponding to the Kolmogorov and Gibson scales bracket key aspects of the experimental data.

Reliable experimental data is exceptionally difficult to procure for strongly transient turbulent flows but remain a prerequisite for a scientific evaluation of different closure elements. The standard manner of evaluating predictive techniques with reference to single parameters, such a pressure rise or propagation velocity, is also insufficient. Furthermore, while visual information is helpful in advancing qualitative understanding, any detailed assessment of controlling mechanisms requires quantitative flow field information. It is therefore a striking deficiency that at the present time only two such data sets exist at meaningful Reynolds numbers [13,14,15,16]. The current work takes advantage of one of these data sets to provide an assessment of the ability of high Damköhler number based approaches to model qualitatively and quantitatively the evolution of a turbulent gaseous explosion in a confined channel. The case considered features a pre-existing turbulence field generated through premixed fuel-air mixture injection at the closed end of a detonation tube [15,16]. In the present work closures at the second moment level are utilized for both velocity and scalar fields. The computational techniques applied are capable of describing phenomena such as flow field anisotropy and of providing qualitatively correct flame dynamics (e.g. Lindstedt & Vaos [17]). The recent developments of comprehensive closures at this level [17,18] is here followed by their application to model a transient multi-dimensional premixed turbulent flame.

GOVERNING EQUATIONS

The aerothermochemical fields are governed by the conservation equations for mass, momentum and scalars cast in a density weighted form. Laminar diffusion terms and external force fields are neglected.

(1) $$\frac{\partial \bar{\rho}}{\partial t} + \frac{\partial \bar{\rho} \tilde{u}_i}{\partial x_i} = 0$$

(2) $$\frac{\partial \bar{\rho} \tilde{u}_i}{\partial t} + \frac{\partial \bar{\rho} \tilde{u}_i \tilde{u}_j}{\partial x_j} = -\frac{\partial \bar{p}}{\partial x_i} - \frac{\partial \bar{\rho} \widetilde{u_i'' u_j''}}{\partial x_j}$$

(3) $$\frac{\partial \bar{\rho} \tilde{c}}{\partial t} + \frac{\partial \bar{\rho} \tilde{u}_j \tilde{c}}{\partial x_j} = -\frac{\partial \bar{\rho} \widetilde{u_j'' c''}}{\partial x_j} + \bar{S}_c$$

In the context of time dependent flows it is important to note that changes in the velocity and scalar fields drives the generation of turbulence and that the feedback is provided though the turbulent correlation terms on the RHS of equations (2,3). The latter are here treated through the corresponding transport equations for the Reynolds stresses (4-6) and scalar fluxes (7-8).

(4) $$\frac{\partial \bar{\rho} \widetilde{u_i'' u_j''}}{\partial t} + \frac{\partial \bar{\rho} \tilde{u}_k \widetilde{u_i'' u_j''}}{\partial x_k} = \frac{\partial \bar{T}_{ij}}{\partial x_k} + P_{ij} + \Phi_{ij} + \phi_{ij} - \bar{\rho} \varepsilon_{ij}$$

The terms on the RHS represent, in order, turbulent transport of the Reynolds stresses, effects of mean strain (or "production" P_{ij}), effects of mean pressure gradients (Φ_{ij}), the turbulent pressure strain term (ϕ_{ij}) and viscous dissipation ($\rho\varepsilon_{ij}$)

(5,6) $$P_{ij} = -\bar{\rho}\left[\widetilde{u_i'' u_k''}\frac{\partial \tilde{u}_j}{\partial x_k} + \widetilde{u_j'' u_k''}\frac{\partial \tilde{u}_i}{\partial x_k}\right] \qquad \Phi_{ij} = -\left[\bar{u}_i''\frac{\partial \bar{p}}{\partial x_j} + \bar{u}_j''\frac{\partial \bar{p}}{\partial x_i}\right] \qquad \phi_{ij} = -\left[\overline{u_i''\frac{\partial p'}{\partial x_j}} + \overline{u_j''\frac{\partial p'}{\partial x_i}}\right]$$

The modelling of the pressure correlation terms in the Reynolds stress equations is the focal point of second moment closures. The terms can be decomposed into redistributive and isotropic parts and details can be found elsewhere (e.g. Lindstedt & Vaos [17]). The latter may be further split into pressure transport and pressure dilation terms. Redistribution terms are invariably modelled by recasting closures (derived on a constant density basis) in a density weighted form and a similar procedure is also applied to the pressure scrambling terms. An algebraic expression for the density weighted fluctuations forming part of the mean pressure gradient term can be derived. The corresponding scalar fluxes for the reaction progress variable are given below.

(7) $$\frac{\partial \bar{\rho} \widetilde{u_j'' c''}}{\partial t} + \frac{\partial \bar{\rho} \tilde{u}_i \widetilde{u_j'' c''}}{\partial x_i} = \frac{\partial \bar{T}_{jc}}{\partial x_i} + P_{jc} + \Phi_{jc} + \phi_{jc} + \overline{u_j'' S_c} - \rho\varepsilon_{jc}$$

(8) $$P_{jc} = -\bar{\rho}\left[\widetilde{u_j'' c''}\frac{\partial \tilde{u}_i}{\partial x_i} + \widetilde{u_i'' u_j''}\frac{\partial \tilde{c}}{\partial x_i}\right] \qquad \Phi_{jc} = -\overline{c''}\frac{\partial \bar{p}}{\partial x_j} \qquad \phi_{jc} = -\overline{c''\frac{\partial p'}{\partial x_j}}$$

The present study considers fully compressible flows with compressibility effects introduced via the solution of a conservation equation for the internal energy and the equation of state. The thermodynamic properties are evaluated from JANAF polynomials and the temperature is calculated via a Newton iteration.

(9) $$\frac{\partial \bar{\rho} \tilde{e}}{\partial t} + \frac{\partial \bar{\rho} \tilde{u}_i \tilde{e}}{\partial x_i} = -\bar{p}\frac{\partial \tilde{u}_i}{\partial x_i} - \frac{\partial \bar{\rho} \widetilde{u_i'' e''}}{\partial x_i} \qquad -\bar{\rho}\widetilde{u_i'' e''} = \frac{\mu_t}{\sigma_t}\frac{\partial \tilde{e}}{\partial x_i} \quad \text{and} \quad PM = \rho RT \quad T = f(c,e)$$

The treatment of flux terms in the internal energy equation presents a currently unresolved challenge and the principal role of Eq. (9) in the present context is to provide a treatment for the calculation of the temperature and density field. The turbulent kinetic energy, required in the evaluation of the "eddy viscosity", is determined from the solution of the Reynolds stress equations and the turbulent Prandtl number is assigned a value of 0.75.

The treatment of the pressure strain terms features a rearrangement into redistributive and isotropic parts with the latter decomposed into pressure transport and dilatation terms.

$$(10) \qquad \phi_{ij}^{R} = -\left[u_i'\frac{\partial p'}{\partial x_j} + u_j'\frac{\partial p'}{\partial x_i} - \frac{2}{3}\delta_{ij}u_i'\frac{\partial p'}{\partial x_i}\right] \quad \phi_{ij}^{T} = -\left[\frac{2}{3}\delta_{ij}\frac{\partial p'u_i'}{\partial x_j}\right] \quad \phi_{ij}^{D} = -\left[\frac{2}{3}\delta_{ij}p'\frac{\partial u_i'}{\partial x_i}\right]$$

The corresponding pressure strain term in the scalar flux equation may be recast in terms of pressure transport (T) and scrambling (S) terms.

$$(11,12) \qquad \phi_{ic}^{T} = -\frac{\partial p'c''}{\partial x_i} \quad \text{and} \quad \phi_{ic}^{S} = -p'\frac{\partial c''}{\partial x_i}$$

The specific model expressions applied are described below.

SPECIFIC MODEL FORMS

The "return to isotropy" and "strain" redistribution parts are obtained from model formulations derived in non-reacting flows. Several suggestions exist at various levels of complexity. The model used here for illustrative purposes is that of Haworth & Pope [19] which is based on a stochastic Lagrangian Generalized Langevin Model (GLM) [20]. The latter features a non-linear return to isotropy and has been calibrated and tested for a range of homogeneous turbulence and free shear flows. An important feature of the model is that it also yields a closure for the pressure scrambling term in the scalar flux equation and thus allows for realizable modelling of both pressure strain correlations. The "return" and "strain" redistribution parts take the following equivalent forms where **b** denotes the anisotropy tensor.

$$(13) \qquad \phi_{ij} = \bar{\rho}\left[\frac{\tilde{\varepsilon}}{\tilde{k}}C_0[\mathbf{b}] + B_{ijkl}[\mathbf{b}]\frac{\partial \tilde{u}_k}{\partial x_l}\right]\tilde{k} = \bar{\rho}\,G_{ik}\,\widetilde{u_k''u_j''} + \bar{\rho}\,G_{jk}\,\widetilde{u_k''u_i''} + \bar{\rho}(C_0 + \frac{2}{3})\delta_{ij}\,\tilde{\varepsilon}$$

The corresponding model form for the scalar flux equation is

$$(14) \qquad \phi_{ic} = \bar{\rho}\left[\frac{\tilde{\varepsilon}}{\tilde{k}}C_0^{c}[\mathbf{b}] + B_{ijk}^{c}[\mathbf{b}]\frac{\partial \tilde{u}_k}{\partial x_l}\right]\widetilde{u_j''c''} = \bar{\rho}\,G_{ik}\,\widetilde{u_k''c''} - \bar{\rho}\frac{\tilde{\varepsilon}_c}{c''^2}\widetilde{u_i''c''}$$

In Eq. (13) the constant C_0 is assigned the value 2.1. The functional form for G_{ij} is linear in the mean velocity gradients and quasi-linear in the anisotropy tensor and the expanded form is given in Appendix A. A number of closures have been suggested for the triple moments. However, the contributions of the diffusion terms to the overall budget of the Reynolds stresses and scalar fluxes is moderate and, consequently, the turbulent transport of the second moments is here modelled using the generalized gradient diffusion model of Daly & Harlow [21].

$$(15,16) \qquad \frac{\partial \bar{T}_{ijk}}{\partial x_i} + \phi_{ijk}^{T} = \frac{\partial}{\partial x_k}\left[C_s\,\bar{\rho}\frac{\tilde{k}}{\tilde{\varepsilon}}\widetilde{u_k''u_l''}\frac{\partial \widetilde{u_i''u_j''}}{\partial x_l}\right] \qquad \frac{\partial \bar{T}_{ick}}{\partial x_i} + \phi_{ick}^{T} = \frac{\partial}{\partial x_k}\left[C_s\,\bar{\rho}\frac{\tilde{k}}{\tilde{\varepsilon}}\widetilde{u_k''u_l''}\frac{\partial \widetilde{u_i''c''}}{\partial x_l}\right]$$

The closure for the dissipation rate of the turbulent kinetic energy is obtained by the standard variable density transport equation model (e.g. [17,22]).

CLOSURE FOR REACTION RATE RELATED TERMS

The closure for the chemical source term presents an interesting problem that entails the determination of an appropriate time scale for scalar turbulence. Traditionally, the closure for the scalar dissipation rate in the high Damköhler number regime is purely based on a constant timescale ratio leading to a direct relation to the mechanical time scale. The analysis is here pursued from the basis of differential models and the form proposed by Jones & Musonge [23] is used here for illustrative purposes.

$$(17) \qquad \frac{\partial \bar{\rho}\tilde{\varepsilon}_c}{\partial t} + \frac{\partial \bar{\rho}\tilde{u}_i\tilde{\varepsilon}_c}{\partial x_i} = \frac{\partial}{\partial x_i}\left[J_i^{\varepsilon_c}\right] + \left[C_1^{\varepsilon_c}\frac{\tilde{\varepsilon}}{\tilde{k}}\frac{P}{\tilde{\varepsilon}} + C_2^{\varepsilon_c}\frac{\tilde{\varepsilon}}{\tilde{k}}\frac{P_c}{\tilde{\varepsilon}_c} - C_3^{\varepsilon_c}\frac{\tilde{\varepsilon}}{\tilde{k}} - C_4^{\varepsilon_c}\frac{\tilde{\varepsilon}_c}{c''^2}\right]\bar{\rho}\tilde{\varepsilon}_c$$

In the above equation, C indicates a model constant, J a turbulent transport term and the production terms (P,P_c) follow from the equations for the evolution of the Reynolds stresses and scalar fluxes. By virtue of Eq. (17) an algebraic expression for the scalar timescale can be derived if it is assumed that the evolution of the scalar dissipation rate is dominated by local source terms. The resulting form reduces to

$$(18) \qquad \left[C_1^{sc}\frac{\widetilde{\varepsilon}}{\widetilde{k}}\frac{P}{\widetilde{\varepsilon}}+C_2^{sc}\frac{\widetilde{\varepsilon}}{\widetilde{k}}\frac{P_c}{\widetilde{\varepsilon}_c}-C_3^{sc}\frac{\widetilde{\varepsilon}}{\widetilde{k}}-C_4^{sc}\frac{\widetilde{\varepsilon}_c}{\widetilde{c}''^2}\right]\cong 0 \quad \text{or} \quad \frac{\widetilde{\varepsilon}_c}{\widetilde{c}''^2}\cong\frac{1}{C_4^{sc}}\left[C_1^{sc}\frac{P}{\widetilde{\varepsilon}}+C_2^{sc}\frac{P_c}{\widetilde{\varepsilon}_c}-C_3^{sc}\right]\frac{\widetilde{\varepsilon}}{\widetilde{k}}=C_1^*\frac{\widetilde{\varepsilon}}{\widetilde{k}}$$

The above procedure may be regarded as typical for the derivation of the commonly adopted scalar time-scale ratio. The obvious requirement is that the sum of the terms in the square bracket does not vary significantly. Perhaps surprisingly, the value for the time scale ratio is typically of order unity for passive scalars in many flows. In cases featuring reactive scalars a similarly derived equation for the scalar dissipation rate includes additional specific terms in the form of correlations between scalar and reaction rate gradients.

$$(19) \qquad \frac{\widetilde{\varepsilon}_c}{\widetilde{c}''^2}=\left[C_1^*+\overline{S}_c^*\right]\frac{\widetilde{\varepsilon}}{\widetilde{k}} \quad \text{where } \overline{S}_c^* = 2D_c\overline{\frac{\partial c''}{\partial x_j}\frac{\partial S_c}{\partial x_j}}$$

Borghi & Mantel [24] have performed a dimensional analysis and show that the above term is proportional to the Damköhler number. It has also been shown by Lindstedt & Vaos [17,18], based on a fractal analysis, that in the latter regime the time scale ratio needs to be modified to account for flame propagation. Bray *et al.* [25] have recently evaluated a number of reaction rate closures in the context of the opposed jet geometry. The conclusions are interesting and suggest that the majority of reaction rate closures fail to predict qualitative trends correctly. Furthermore, it has been shown that irrespective of the level of closure adopted – algebraic or transport equation based – current models could generally not be calibrated to perform satisfactorily irrespective of the choice of modelling constant(-s). An exception was found to be the fractal based closure derived by Lindstedt & Sakthitaran [26] and discussed further by Lindstedt & Vaos [17]. It must, however, be recognized that Bray *et al.* [25] also in this case show that there is a significant uncertainty relating to the appropriate modelling constant and that the value proposed [17] appears too low. Based on the above considerations the resulting modified expression for the time scale ratio is proposed.

$$(20) \qquad \frac{\widetilde{\varepsilon}_c}{\widetilde{c}''^2}=\left[C_1^*+C_2^*\frac{\rho_0}{\overline{\rho}}\frac{u_l}{v_k}\right]\frac{\widetilde{\varepsilon}}{\widetilde{k}}=\left[C_1^*+C_2^*\frac{1}{\overline{\rho}}\frac{\sqrt{(\mu/\sigma_{Y_c})R_cM_c}}{v_k}\right]\frac{\widetilde{\varepsilon}}{\widetilde{k}}$$

The reaction rate (R_cM_c) is the integral across the corresponding (laminar) flame sheet and the viscosity (μ) and Prandtl number (σ_c) refer to the corresponding laminar properties evaluated at some inner reference plane. It is important to note that the above expression implies that burning velocity reductions at high Reynolds numbers are due to partial flame quenching and not to flame geometry related considerations. The limitations of the above derivation procedure and the resulting expression are obvious but to a large degree identical to those present in standard modelling approaches. From a practical perspective, however, the derived form ensures a consistent scaling behaviour for turbulent burning velocities in the high Damköhler number regime of combustion. For the present case, the constant C_1^* has been assigned the standard value of 1 while the parameter C_2^* has been calibrated to the value of 1.2 on the basis of flames stabilized in an opposed jet geometry. The corresponding reaction rate expression follows from the assumption of a bimodal PDF.

$$(21) \qquad \overline{S}_c=\overline{\rho}C_R\frac{\widetilde{\varepsilon}_c}{\widetilde{c}''^2}\widetilde{c}(1-\widetilde{c})\cong\overline{\rho}C_R\left[C_1^*+C_2^*\frac{\rho_0}{\overline{\rho}}\frac{u_l}{v_k}\right]\frac{\widetilde{\varepsilon}}{\widetilde{k}}\widetilde{c}(1-\widetilde{c})$$

The reaction rate constant C_R is assigned the value of 3.5 [27] and the above expression arguably constitutes an upper limit. The velocity reaction rate correlation term is here closed through the assumption of a bimodal PDF [17].

$$(22) \qquad -\overline{\rho}\frac{\widetilde{\varepsilon}_c}{\widetilde{c}''^2}\overline{u_i''c''}+\overline{u_i''S_c}=\frac{\overline{S}_c}{\widetilde{c}''^2}\left(\frac{1}{2}-\widetilde{c}\right)$$

Different models for the pressure dilation term have been proposed by Lindstedt & Hulek [28] and Zhang & Rutland [29]. The former suggestion has the virtue of being consistent with the assumed thermochemical conditions and, while the latter is heuristic in nature, it does not present problems in terms of realizability. In the present work the term has been omitted as the influence is not expected to be large [28].

EXPERIMENTAL AND COMPUTATIONAL CONFIGURATION

The transition of a turbulent flame to a gaseous explosion in a confined pre-existing turbulent flow field is considered in the context of the data set produced by Lindstedt & McCann [15,16]. The configuration yields over-pressures of around 200 kPa and peak bulk velocities around 400 m/s – both significantly higher than those reported by Lindstedt & Sakthitharan [13,14] for initially quiescent mixtures – and the turbulence velocities reach values of the order 40 m/s. Deflagration to detonation transition occurs in the same configuration for more reactive mixtures than the stoichiometric methane-air case reported here. The detonation tube features six interchangeable rectangular sections (72 mm x 34 mm) of length 1.825 m and two window sections of length 0.385 m. Initial turbulence is generated by an axi-symmetric jet of 5 mm internal diameter centred in a plate at the ignition end of the flame tube. The flow field created by the injection of the premixed fuel-air mixture has been measured [15] and the data is here used in order to form the initial set of conditions. Ignition is obtained by two opposing electrodes placed symmetrically either side of the jet centre line. A 5 mm thick obstacle with a height of 36 mm is placed downstream of the jet exit at a distance of 415 mm. The closure outlined above is here applied to the above geometry using a locally refined two-dimensional computational grid (~ 100 000 nodes) sufficient to provide a grid independent solution. The computations feature a second order TVD scheme and an implicit predictor-corrector method with time splitting error control [11,17].

The applied diagnostics include sixteen coaxial ionisation probes, used to detect flame arrival times, and six piezoelectric pressure transducers positioned along the channel. The flame propagation process was also visualised by means of spark schlieren photography featuring a parallel beam of white light. Velocities were obtained using the standard dual-beam forward scatter laser Doppler anemometer arrangement and the data reduction technique reported by Lindstedt & Sakthitharan [13] applied. Velocity measurements along the axial (u–velocity) and vertical directions (v–velocity) have been obtained at 33 points above and downstream of the obstacle. All the points lie on the vertical plane passing through the axis of the flame tube. Sakthitharan [14] has shown, through flow field measurements across the detonation tube, that the flow is predominantly two-dimensional in the region close to the obstacle. Although there are temporal variations associated with the initial kernel growth (~ 10 %), the reproducibility of the flame arrival at subsequent ports is excellent with comparatively small variations (~ 3 %). The latter indicates that the development of the vortex structure downstream of the baffle is highly reproducible and relatively insensitive to initial variations. Problems do naturally arise with measurements of mean and, in particular, turbulence velocities in the current strongly accelerated flow. It is therefore expected that the measurement accuracy is significantly reduced following the onset of the explosion.

RESULTS AND DISCUSSION

Computed flame contours are compared with schlieren images in Figs. 1 and 2. The relative times in the flame propagation cycle are close but not matched exactly and, furthermore, the schlieren images are "line-of-sight" across the flame tube. Caution is therefore required in interpreting the images. However, it is seen that the creation of large scale flame folds and the flame wrapping into the vortex are qualitatively reproduced by the computation. Clearly the flow features large scale instabilities along with strong turbulence generation in the shear layer and re-circulation zone behind the obstacle. The large scale instabilities are of order 10 mm with the wrinkling of the flame appearing to be of order 1 mm. The predicted pressure traces are compared with measurements in Fig. 3a-b. Close to the ignition point the agreement is very satisfactory as shown in Fig. 3a. However, it is also evident that peak pressures are somewhat under-predicted closer to the obstacle (Fig. 3b), though the shape of the pressure trace profile remains comparatively well reproduced.

Further evidence that the predictions are qualitatively good and quantitatively reasonable can be found in the axial and cross-stream mean velocity profiles shown in Figs. 4 and 5 for the plane where the obstacle is located. The interaction of strong flow gradients in the *vena contracta* over the baffle with the explosion generated pressure pulses are exceptionally difficult to measure and it is likely that the experimental data underestimates the peaks in the bulk velocities. However, with the exception of the latter, the profile shapes and magnitudes are well reproduced for the axial (u) velocity component. The computations show strong oscillations in the burnt gas due to travelling pressure waves (evident in the pressure traces shown in Figs. 3) which clearly could not be captured by the measurements. The agreement for the cross-stream (v) component is much less satisfactory. However, it can be noted that the flow velocities range from well in excess of 100 m/s close to the obstacle tip (42 mm) to around 10 m/s closer (10 mm) to the top wall. It may further be noticed that mean velocities are well reproduced until the onset of the explosion. Further away from the obstacle, at the 515 mm plane, the agreement between measurements and computations is generally satisfactory for the axial velocity component as shown in Fig. 6. However, it may be noted that the strongest flow accelerations again present what probably is measurement difficulties. The qualitative and quantitative agreement for the cross-stream velocity component is very satisfactory as shown in Fig. 7 - despite the fact that the time evolution of the flow is extremely complex. It may also be noted that the flow acceleration is less severe in the cross-stream direction and hence greater confidence may be placed in experimental data.

The difficulties outlined above in the context of the determination of the bulk velocity field are naturally also present in the measurements of the turbulence intensities. It is important to note that the vortex shedding and bulk flow instabilities do not satisfy the common criteria (e.g. irregularity) associated with turbulence (e.g. Tennekes & Lumley [30]). A scale separation associated with bulk and turbulent motion is evidently present in the current flow but becomes awkward to analyse both computationally and experimentally. The combination of a time window of 500 μs, used experimentally in order to gather sufficient statistics, along with the difficulties experienced by seeding particles in following flow, renders the measurements difficult to interpret. Nevertheless, up to the point of the onset of the explosion (~ 16-17 ms) there is fair agreement between computed and measures values of the axial component as shown in Fig. 8. Following the onset of the explosion the axial turbulence velocities – in particular – are very strongly affected and it is not possible to advance conclusions regarding the agreement between computed and measured values. The cross-stream velocity component is again much less affected and remains surprisingly well reproduced both qualitatively and quantitatively as shown in Fig. 9. A comparison of the results shown in Figs. 7 and 9 is interesting and suggests that despite the difficulties associated with both measurements and computations the overall agreement is encouraging. It is notable that the rapid changes in the velocity field and the resulting turbulence generation are both well captured. Perhaps surprisingly, the results indicate that the computational results are in many cases close to experimental uncertainties for the current exceptionally complex flow.

CONCLUSIONS

The ability to model the formation and evolution of DDT kernels is of fundamental importance to a range of practical applications such as pulsed detonation engines. In order to advance the subject it is necessary to explore the sensitivity of the overall phenomena to the major closure elements of physical relevance to the problem. Experimental work has shown that in many practical areas the driving force for the transition can be found in the interaction of turbulence and chemistry, while in other cases it will reside with shock (turbulent) boundary layer interactions. Both topics present similar – if not close to identical – modelling difficulties irrespective of the technique used for the flow field (e.g. LES or unsteady RANS). Nevertheless, it is naturally essential that a sensible reproduction of the flow field is achieved by the computational method of choice. In the absence of experimental data such assessments are conjectural and the present work has used comparatively detailed data for turbulent gaseous explosion as a basis for comparisons. The experimental data set is naturally subject to significant uncertainties resulting from exceptionally difficult measurement conditions resulting from repeated

flow acceleration/deceleration cycles. Despite such difficulties the work has shown that the application of comprehensive higher moment closures to the modelling of the initial onset of DDT is technically possible and, furthermore, results in encouraging quantitative and qualitative agreement with measurements. It may be of interest to note that good agreement for other unsteady flows have also been obtained (e.g. Durbin [33]) using moment based methods. The turbulence chemistry interactions can in principle be closed using a transported PDF approach combined with comprehensive auto-ignition chemistry. It is, however, likely that the scalar space required will be of order 20 species even for comparatively simple fuels (e.g. Lindstedt *et al.* [31] and Pope *et al.* [32]) and, accordingly, the computational requirements are exceptional. The current finding is interesting as it suggests that improved closures for turbulence-chemistry interactions combined with the relative economy of unsteady RANS calculations may provide a route towards the modelling of obstacle/wall enhanced turbulence induced transition to detonation.

Acknowledgement

The authors wish to gratefully acknowledge the financial support of the EOARD under contract F61775-01-We 050 and the encouragement of Dr. F Schauer, Dr. C. Raffoul, Dr. P. Ouzts and Dr. G.D. Roy. The assistance of Miss S. Louloudi in typing some of the equations is also gratefully acknowledged.

References

[1] Roy, G.D. "Pulsed Detonation Phenomena for Air Breathing Propulsion", Invited Lecture, 14th International Symposium on Air Breathing Engines, *ISABE Paper 99-7127* (1999).

[2] Kailasanath, K. "A Review of PDE Research – Performance Estimates", AIAA 2001 – 0474.

[3] Tishkoff, J.M., Drummond, J.P., Edwards, T. and Nejad, A.S. 'Future Direction of Supersonic Combustion Research: Air Force/NASA Workshop on Supersonic Combustion', *AIAA 97-1017* (1997).

[4] Lindstedt, R.P. and Michels, H.J. "Lindstedt, R.P. and Michels, H.J., "Deflagration to Detonation Transition in Alkane, Alkene Mixtures with O_2/N_2", *Combustion and Flame*, 72:63-72 (1988).

[5] Lindstedt, R.P. and Michels, H.J. "Deflagration to Detonation Transitions and Strong Deflagrations in Alkane and Alkene Mixtures with Air", *Combustion and Flame* 76:169 – 182 (1989).

[6] Arntzen, B.J., Hjertager, B., Lindstedt, R.P., Merex, W.P.M. and Popat, N. "Investigations to Improve and Assess the Accuracy of Computational Fluid Dynamic Based Explosion Models", *Journal of Hazardous Materials* 45:1-25 (1995).

[7] Hulek, T. and Lindstedt, R.P. 'Computations of Steady-State and Transient Premixed Turbulent Flames using Transported PDF Methods', *Combustion and Flame* 104:481-504 (1996).

[8] Hulek, T. and Lindstedt, R.P. "Joint Scalar-Velocity pdf Modelling of Finite Rate Chemistry in a Scalar Mixing Layer", *Combustion, Science and Technology* 136:303-332 (1998).

[9] Lindstedt, R.P. and Vaos, E.M. 'Modeling of Mixing Processes in Non-Isothermal and Combusting Flows', *Advances in Turbulence VII*, ISBN 84-89925-65-8, (2000), pp. 493 – 496.

[10] Lindstedt, R.P. and Kuan, T.S. 'Prediction of Steady and Transient Bluff Body Stabilized Flames', Proceedings of the 6th International Workshop on Measurements and Computations of Turbulent Nonpremixed Flames, July 2002, http://www.ca.sandia.gov/tdf/Workshop.html

[11] Catlin, C.A. and Lindstedt, R.P., "Premixed Turbulent Burning Velocities Derived from Mixing Controlled Reaction Models with Cold Front Quenching", *Combustion and Flame* 85:427-439 (1991).

[12] Colangelo, G. and Lindstedt, R.P. "Higher Moment Based Modeling of Turbulence Enhanced DDT Kernels in Confined Fuel-Air Mixtures', in Advances in Confined Detonations, ed. G.D. Roy, S.M. Frolov, R.J. Santoro, and S.A. Tsyganov, ISBN 5-94588-008-8, Torus Press Ltd, pp. 3 -12 (2002).

[13] Lindstedt, R.P. and Sakthitharan, V., "Time Resolved Velocity and Turbulence Measurements in Turbulent Gaseous Explosions", *Combustion and Flame* 114:469-483 (1998).

[14] Sakthitharan, V. "Time-Resolved Measurements of Flame Propagation over Baffle-Type Obstacles", Ph.D. Thesis, Imperial College of Science, Technology and Medicine, 1995.

[15] McCann, H.A. "Time Resolved Measurements of Propagating Turbulent Flames", Ph.D. Thesis, Imperial College of Science, Technology and Medicine, 1997.

[16] Lindstedt, R.P. and McCann, H.A. "Time Resolved Flow Characteristics of Confined Turbulent Gaseous Explosions". Presented at the 18th ICDRS Meeting Seattle, August 2001.

[17] Lindstedt, R.P. and Vaos, E.M. 'Modelling of Premixed Turbulent Flames with Second Moment Methods', *Combustion and Flame* 116:461-485 (1999).

[18] Lindstedt, R.P. and Vaos, E.M. 'Second Moment Modelling of Premixed Turbulent Flames Stabilised in Impinging Jet Geometries', *Twenty-Seventh Symposium (International) on Combustion/The Combustion Institute*, Pittsburgh, (1998), pp. 957-962.

[19] Haworth, D.C. and Pope, S.B. 'A PDF Modeling Study of Self-Similar Turbulent Free Shear Flows', *Phys. Fluids* 30:1026-1044 (1987).

[20] Haworth, D.C. and Pope, S.B. 'A Generalized Langevin Model for Turbulent Flows', *Phys. Fluids* 29:387-405 (1986).

[21] Daly, B.J. and Harlow, F.H. 'Transport Equations in Turbulence', *Phys. Fluids* 13:2634-2649 (1970)

[22] Jones, W.P. 'Turbulence Modelling and Numerical Solution Methods for Variable Density and Combusting Flows', *in Turbulent Reacting Flows*, Academic Press, pp. 309-374 (1993).

[23] Jones, W.P. and Musonge, P. 'Closure of Reynolds Stress and Scalar Flux Equations' *Phys. Fluids* 32:3589-3604 (1988)

[24] Borghi, R. and Mantel, T. 'A New Model of Premixed Wrinkled Flame Propagation Based on a Scalar Dissipation Equation", *Combustion and Flame* 96:443-457 (1994).

[25] Bray, K.N.C., Champion, M. and Libby, P.A. Pre-mixed Flames in Stagnation Turbulence. Part V - Evaluation of Models for the Chemical Source Term. *Combustion and Flame* 127:2023-2040 (2001).

[26] Lindstedt, R.P. and Sakthitharan, V. 'Modelling of Compressible Turbulent Reacting Flows', Presented at Eight Symposium on Turbulent Shear Flows, Technical University of Munich, 1991.

[27] Vaos, E.M. 'Second Moment Methods for Turbulent Flows with Reacting Scalars', *PhD Thesis*, Imperial College of Science, Technology and Medicine, 1998.

[28] Hulek, T. and Lindstedt, R.P. 'Modelling of Unclosed Non-linear Terms in a *pdf* Closure for Turbulent Flames', *Journal of Mathematical and Computer Modelling*, 24:137-147 (1996).

[29] Zhang, S. and Rutland, C.J. 'Premixed Flame Effects on Turbulence and Pressure Related Terms', *Combustion and Flame* 102:447-461 (1995)

[30] Tennekes, H. & Lumley, J.L. 'A First Course in Turbulence', MIT Press (1972).

[31] Lindstedt, R.P., Louloudi, S. and Vaos, E.M. 'Transported PDF Modeling of Pollutant Emissions in Turbulent Jet Flames with Comprehensive Chemistry', *Proceedings of the Combustion Institute* 28, (2000), pp. 149-156.

[32] Tang, Q., Xu, J. and Pope, S.B. 'Probability Density Function Calculations of Local Extinction and NO Production in Piloted-Jet Turbulent Methane-Air Flames', *Proceedings of the Combustion Institute* 28, (2000), pp. 133-139.

[33] Durbin, P.A. 'Separated Flows Computations with the k-ε-v^2 Model', AIAA Journal 33:659-664 (1995).

APPENDIX A

The formulations resulting from the GLM [19,20] for the Reynolds stresses and scalar fluxes are given above. The G_{ij} tensor has the following form:

$$G_{ij} = \frac{\tilde{\epsilon}}{\tilde{k}}\left(\alpha_1\delta_{ij} + \alpha_2 b_{ij}\right) + H_{ijkl}\frac{\partial \tilde{u}_k}{\partial x_l}$$

where

$$H_{ijkl} = \beta_1\delta_{ij}\delta_{kl} + \beta_2\delta_{ik}\delta_{jl} + \beta_3\delta_{il}\delta_{jk}$$
$$\gamma_1\delta_{ij}b_{kl} + \gamma_2\delta_{ik}b_{jl} + \gamma_3\delta_{il}b_{jk}$$
$$\gamma_4\delta_{kl}b_{ij} + \gamma_5\delta_{jl}b_{ik} + \gamma_6\delta_{jk}b_{il}$$

The model contains 11 coefficients of which 6 can be eliminated by exact constraints deduced form the Navier-Stokes equations. The remaining 5 were assigned values by matching experimental data [19] and no adjustment made in the present work.

$$\alpha_2 = 3.78 \qquad \beta_1 = -0.2 \qquad \beta_2 = 0.8 \qquad \beta_3 = -0.2$$
$$\gamma_1 = 0.0 \qquad \gamma_2 = 1.04 \qquad \gamma_3 = -0.34$$
$$\gamma_4 = 0.0 \qquad \gamma_5 = 1.99 \qquad \gamma_6 = -0.76$$

$$\alpha_1 = -\left[\frac{1}{2} + \frac{3}{4}C_0 + \alpha_2 b_{ij}^2 + \left(\beta_2 + \beta_3 + \frac{1}{3}\gamma^*\right)I_1 + \gamma^* I_2\right]$$

where

$$\gamma^* = \gamma_2 + \gamma_3 + \gamma_5 + \gamma_6$$

$$I_1 = b_{ij}S_{ij}^* \qquad S_{ij}^* = \frac{1}{2}\frac{\tilde{k}}{\tilde{\epsilon}}\left[\frac{\partial \tilde{u}_i}{\partial x_j} + \frac{\partial \tilde{u}_j}{\partial x_i}\right]$$

$$I_2 = b_{ij}^2 S_{ij}^* \qquad b_{ij}^2 = b_{ik}b_{kj}$$

$$\mathbf{b} = b_{ij} = \frac{\tilde{u_i''}\tilde{u_j''}}{\tilde{u_k''}\tilde{u_k''}} - \frac{\delta_{ij}}{3}$$

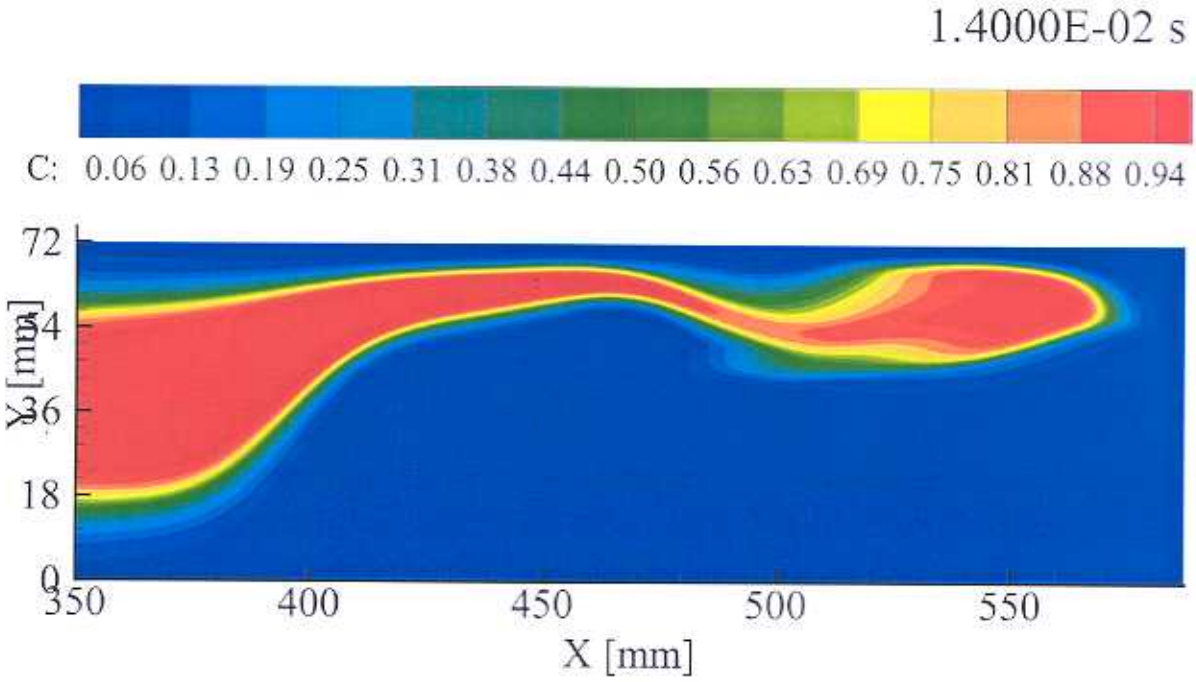

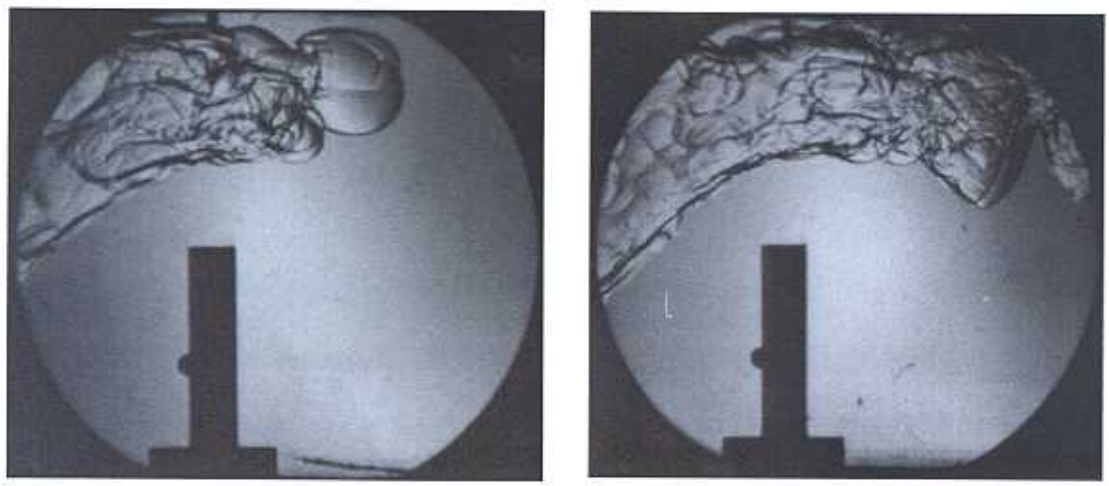

Figure 1. Comparison of computed and measured flame images around the time the flame moves past the obstacle. The computation shows a later time and the schlieren images illustrate the process leading up to the formation of the large scale structures.

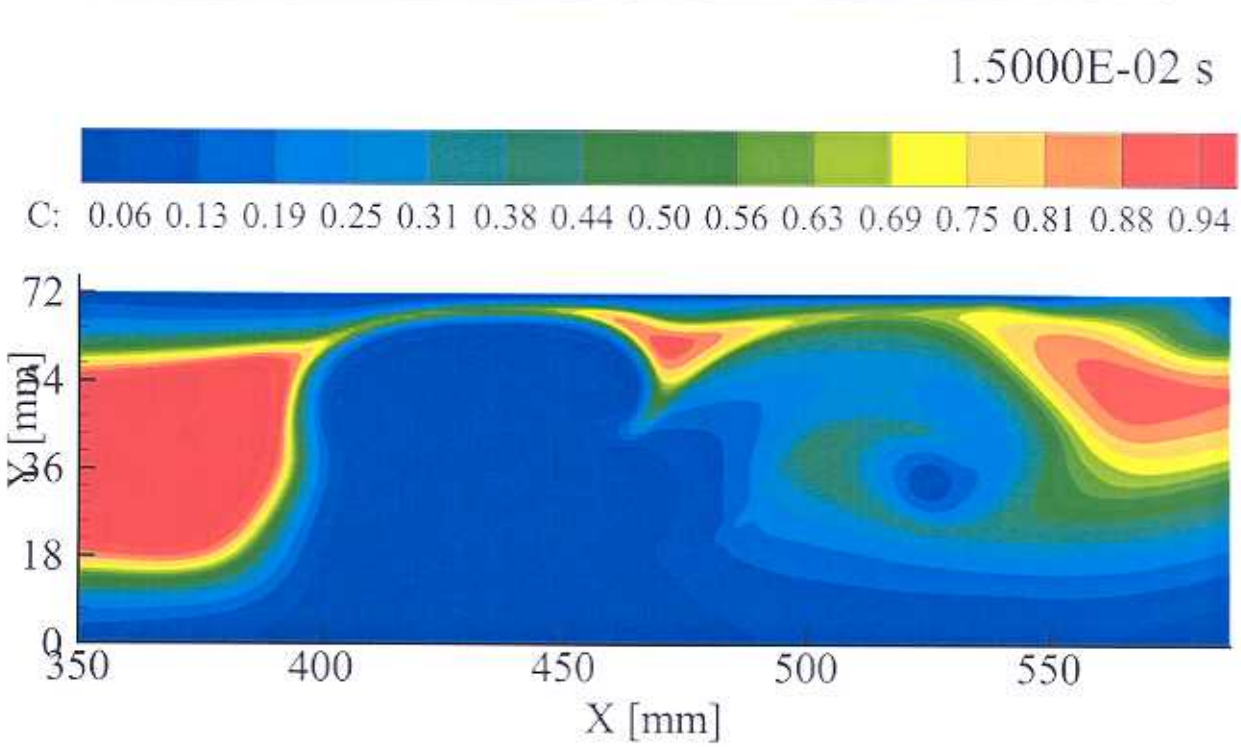

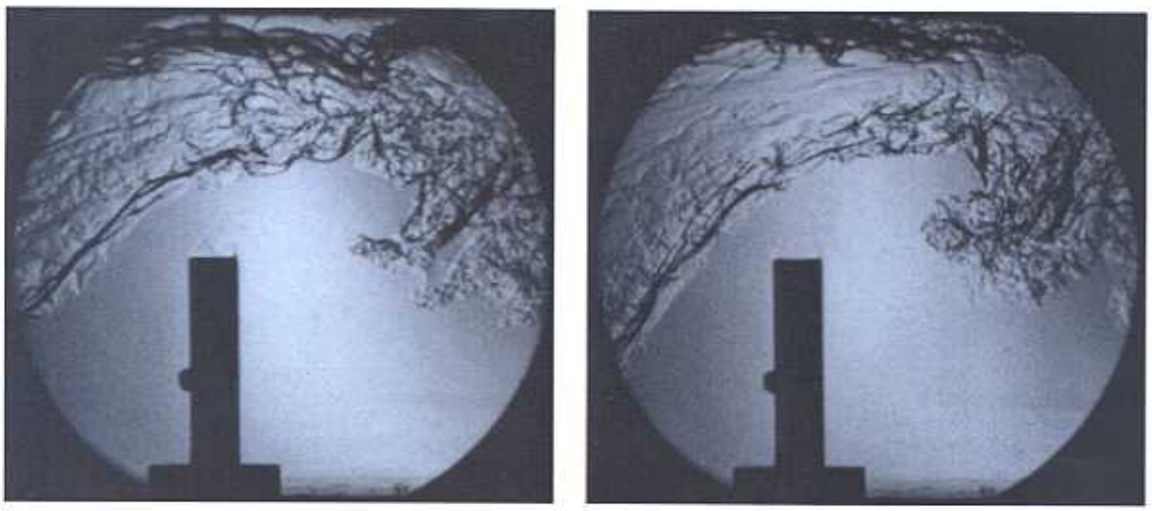

Figure 2. Comparison of experimental and computed flame images at later times. Both the computations and the measurements clearly show large scale instabilities propagating downstream of the obstacle. The experimental images show the superimposed turbulent flame wrinkling. The large scale instabilities appear to be of order 10^{-2} m and the flame wrinkling of order 10^{-3} m.

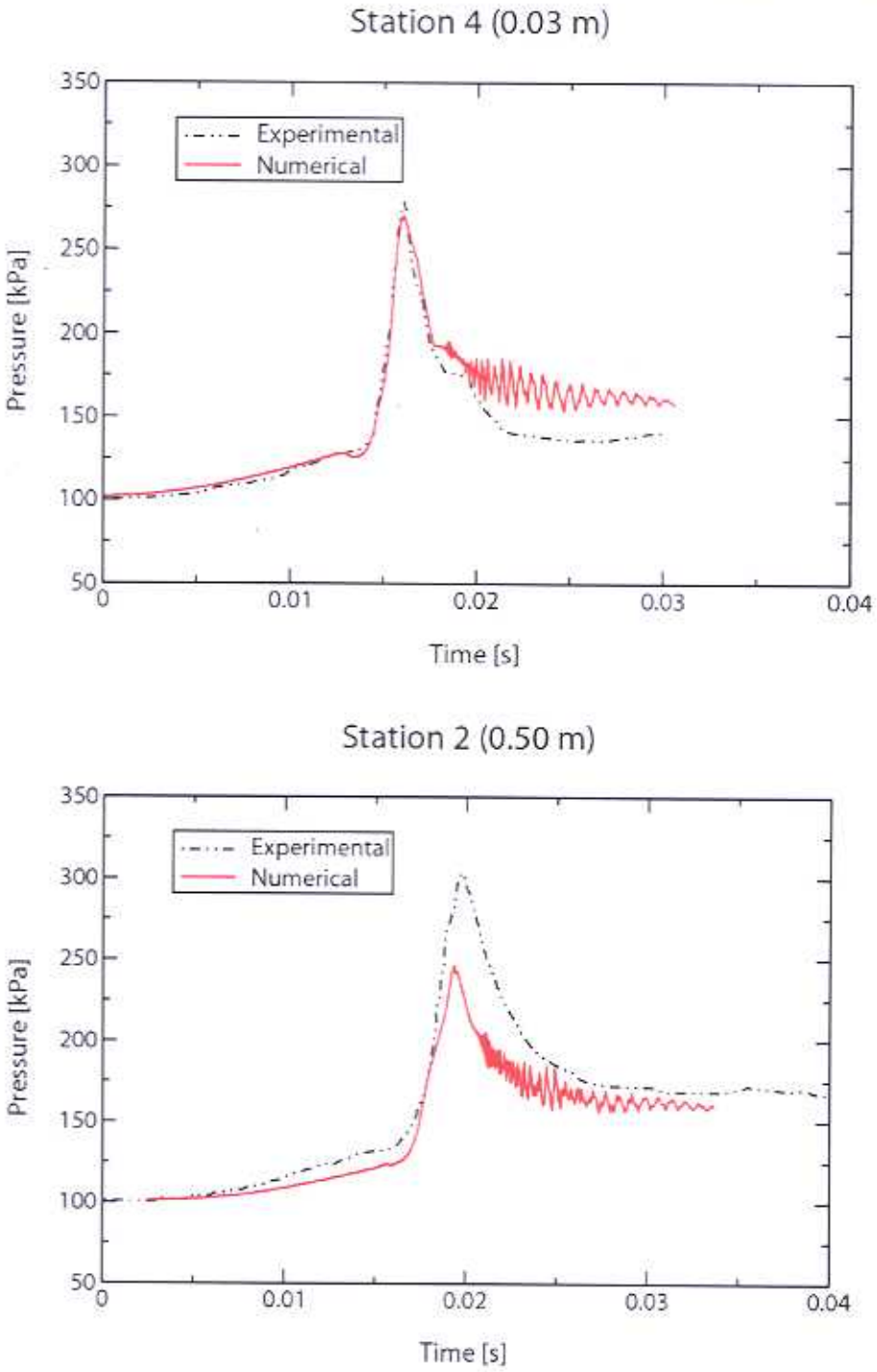

Figure 3. Comparison of computed and measured pressure traces for a turbulent gaseous explosion in a pre-existing turbulence field. The figures show the pressure traces on both sides of the obstacle.

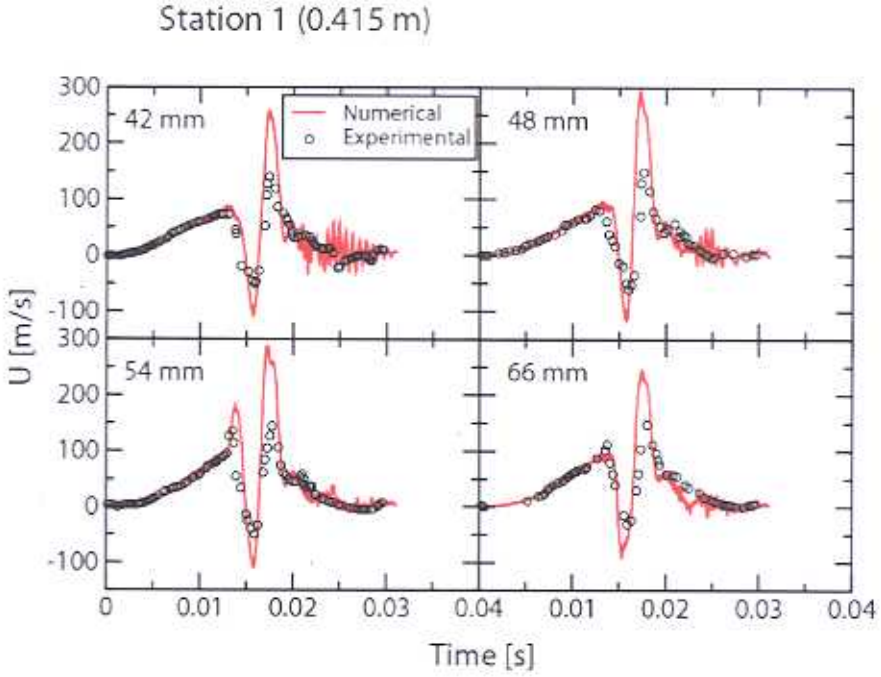

Figure 4. Comparison of computed and measured axial mean velocities at 4 measuring stations along the 415 mm plane (directly above the obstacle) for a turbulent gaseous explosion in a pre-existing turbulence field.

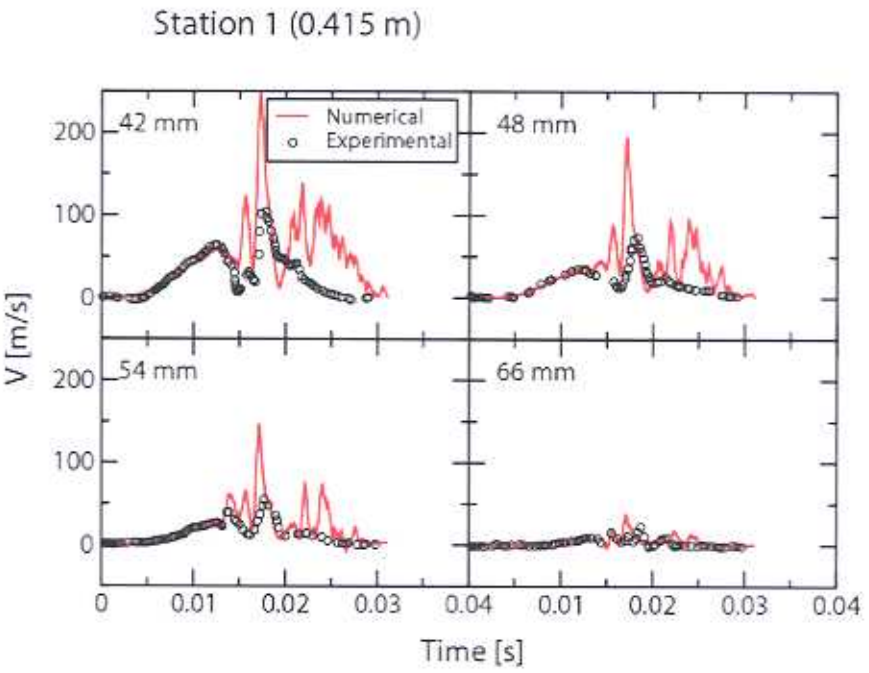

Figure 5. Comparison of computed and measured cross stream mean velocities at 4 measuring stations along the 415 mm plane (directly above the obstacle) for a turbulent gaseous explosion in a pre-existing turbulence field.

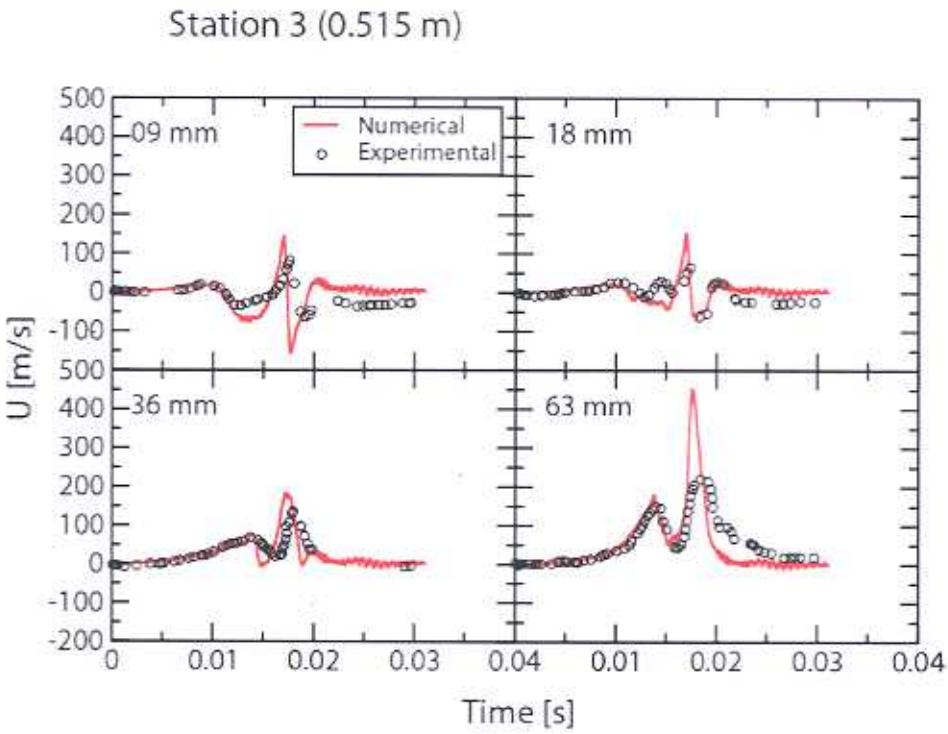

Figure 6. Comparison of computed and measured axial mean velocities at 4 measuring stations along the 515 mm plane (100 mm downstream of the obstacle) for a turbulent gaseous explosion in a pre-existing turbulence field.

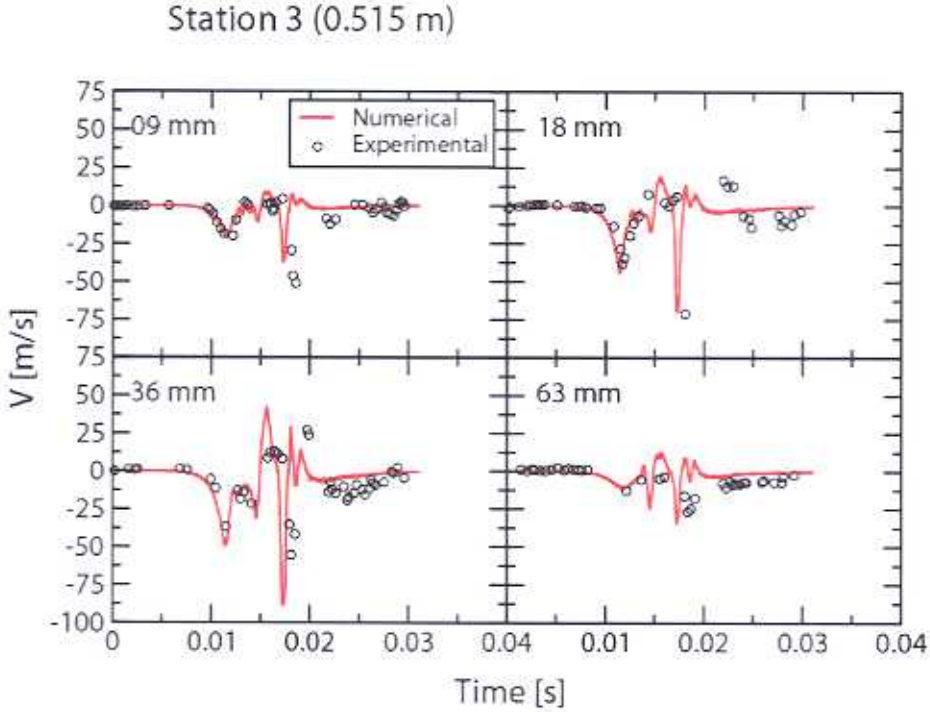

Figure 7. Comparison of computed and measured cross stream mean velocities at 4 measuring stations along the 515 mm plane (100 mm downstream of the obstacle) for a turbulent gaseous explosion in a pre-existing turbulence field.

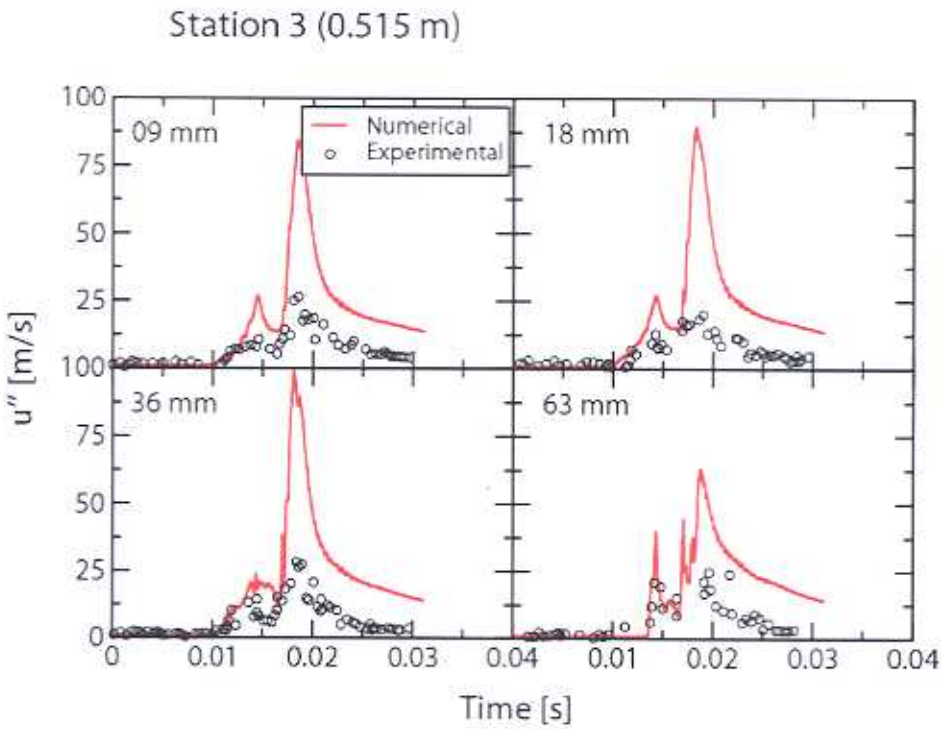

Figure 8. Comparison of computed and measured axial turbulence velocities at 4 measuring stations along the 515 mm plane (100 mm downstream of the obstacle) for a turbulent gaseous explosion in a pre-existing turbulence field.

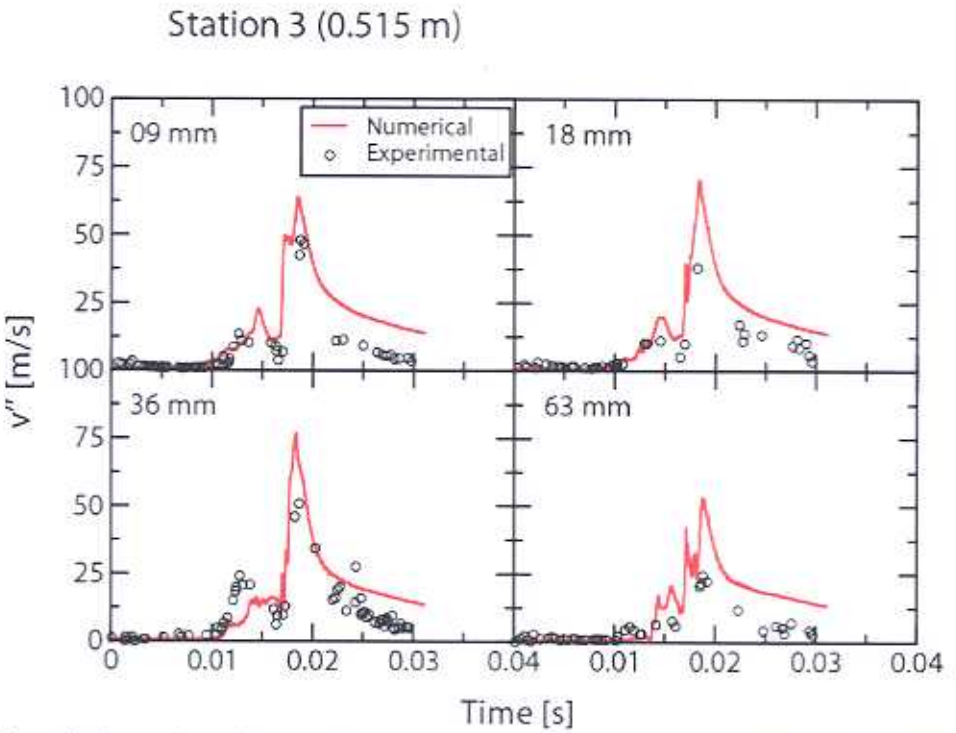

Figure 9. Comparison of computed and measured cross stream turbulence velocities at 4 measuring stations along the 515 mm plane (100 mm downstream of the obstacle) for a turbulent gaseous explosion in a pre-existing turbulence field.